# UC Irvine
## UC Irvine Previously Published Works


### Title
Astrocytic Ephrin-B1 Controls Excitatory-Inhibitory Balance in Developing Hippocampus


### Permalink
https://escholarship.org/uc/item/7ww86793



### Journal
Journal of Neuroscience, 40(36)

### ISSN
0270-6474



### Authors
Nguyen, Amanda Q
Sutley, Samantha
Koeppen, Jordan
et al.



### Publication Date
2020-09-02

### DOI
10.1523/jneurosci.0413-20.2020

Peer reviewed



eScholarship.org Powered by the California Digital Library
University of California

# Astrocytic ephrin-B1 controls excitatory-inhibitory balance in developing hippocampus

Running title: Astrocytic ephrin-B1 in synapse development

Amanda Q Nguyen[1, 2], Samantha Sutley[1], Jordan Koeppen[1, 3], Karen Mina[1], Simone Woodruff[1], Sandy Hanna[1], Alekya Vengala[1], Peter W Hickmott[2,4], Andre Obenaus[5], Iryna M Ethell[1, 2, 3*]

[1]*Division of Biomedical Sciences, University of California Riverside School of Medicine, Riverside, California 92521, United States*

[2]*Neuroscience Graduate Program, University of California Riverside, Riverside, California 92521, United States*

[3]*Cell, Molecular, and Developmental Biology Graduate program, University of California Riverside, California 92521, United States*

[4]*Department of Psychology, University of California Riverside, Riverside, California 92521, United States*

[5]*Department of Pediatrics, University of California Irvine, Irvine, California 92350, United States*

*Corresponding author:
Iryna M. Ethell, PhD
Division of Biomedical Sciences
University of California Riverside School of Medicine,
Riverside, California 92521, USA
iryna.ethell@medsch.ucr.edu

**Pages: 55**
**Figures: 8**
**Abstract (250 words); Introduction (658 words); Discussion (1,640 words)**

**Conflict of Interest:** The authors declare no competing financial interests.

**Acknowledgements:** The authors thank members of Drs. Ethell, Obenaus and Hickmott laboratories for helpful discussions and comments. We also thank Arnold Palacios, Dr. Roman Vlkolinsky, Emil Rudobeck, Jeffrey Rumschlag, Micah Feri, Alexander King and Mary Hamer for technical support, and David Carter for advice on confocal microscopy. Research was supported by MH67121 grant from NIMH (IE) and 1S10OD020042-01 grant from the Research Infrastructure Programs of the NIH. The authors declare no competing financial interests.

**Abstract**

Astrocytes are implicated in synapse formation and elimination that are associated with developmental refinements of neuronal circuits. Astrocyte dysfunctions are also linked to synapse pathologies associated with neurodevelopmental disorders and neurodegenerative diseases. Although several astrocyte-derived secreted factors are implicated in synaptogenesis, the role of contact-mediated glial-neuronal interactions in synapse formation and elimination during development is still unknown. In this study, we examined whether the loss or overexpression of the membrane-bound ephrin-B1 in astrocytes during postnatal day (P) 14-28 period would affect synapse formation and maturation in the developing hippocampus. We found enhanced excitation of CA1 pyramidal neurons in astrocyte-specific ephrin-B1 knock-out (KO) male mice, which coincided with a greater vGlut1/PSD95 co-localization, higher dendritic spine density and enhanced evoked AMPAR and NMDAR excitatory postsynaptic currents (EPSCs). In contrast, EPSCs were reduced in CA1 neurons neighboring ephrin-B1 overexpressing astrocytes. Overexpression of ephrin-B1 in astrocytes during P14-28 developmental period also facilitated evoked inhibitory postsynaptic currents (IPSCs) in CA1 neurons, while evoked IPSCs and miniature IPSC (mIPSC) amplitude were reduced following astrocytic ephrin-B1 loss. Lower numbers of parvalbumin (PV)-expressing cells and a reduction in the inhibitory VGAT/Gephyrin-positive synaptic sites on CA1 neurons in the SP and SO layers of KO hippocampus may contribute to reduced inhibition and higher excitation. Finally, dysregulation of excitatory/inhibitory (E/I) balance in KO male mice is most likely responsible for impaired sociability observed in these mice. The ability of astrocytic ephrin-B1 to influence both excitatory and inhibitory synapses during development can potentially contribute to developmental refinement of neuronal circuits.

**Significance Statement:**

This report establishes a link between astrocytes and the development of E/I balance in the mouse hippocampus during early postnatal development. We provide new evidence that astrocytic ephrin-B1 differentially regulates development of excitatory and inhibitory circuits in the hippocampus during early postnatal development using multidisciplinary approach. The ability of astrocytic ephrin-B1 to influence both excitatory and inhibitory synapses during development can potentially contribute to developmental refinement of neuronal circuits and associated behaviors. Given widespread and growing interest in the astrocyte-mediated mechanisms that regulate synapse development, and the role of EphB receptors in neurodevelopmental disorders, these findings establish a foundation for future studies of astrocytes in clinically relevant conditions.

## Introduction

Synapses are the building blocks of neuronal networks functioning as fundamental information-processing units in the brain (Südhof and Malenka, 2008; Mayford et al., 2012). Excitatory glutamatergic synapses are specialized cell-cell connections that facilitate neuronal activity, which is also fine-tuned by a complex network of inhibitory inputs from γ-aminobutyric acid (GABA) containing interneurons. Activity-mediated formation, pruning and maturation of specific synapses are important in establishing neural circuits. Improper synapse development that leads to imbalance between excitatory and inhibitory (E/I) synaptic activity is linked to several neurologic disorders, including autism spectrum disorders (ASD; (Gao and Penzes, 2015; Lee et al., 2017) and epilepsy (Fritschy, 2008; Bonansco and Fuenzalida, 2016). Thus, investigations of the mechanisms underlying excitatory and inhibitory synapse development may contribute to an understanding of the pathophysiological mechanisms of these brain disorders.

Astrocytes are able to control the neuronal circuits by regulating the formation, pruning, and maturation of synapses. Astrocyte-secreted factors, such as thrombospondin (Christopherson et al., 2005), hevin (Kucukdereli et al., 2011) and glypican (Allen et al., 2012), are known to promote synaptogenesis; whereas the release of gliotransmitters such as glutamate (Fellin et al., 2004), D-serine (Henneberger et al., 2010), and TNF-α (Beattie et al., 2002; Stellwagen and Malenka, 2006) can modulate synaptic functions. Astrocytic processes are also suggested to modulate synapse number and function through direct contact with dendritic spines and presynaptic boutons (Araque et al., 1999; Ullian et al., 2001; Hama et al., 2004; Clarke and Barres, 2013; Allen and Eroglu, 2017, Chung et al., 2013).

EphB receptor tyrosine kinases and their ephrin-B ligands are membrane-associated proteins that play an important role in regulating cell-cell interactions during development

including axon guidance (Zimmer et al., 2003), spinogenesis and synaptogenesis (Dalva et al., 2000; Ethell et al., 2001; Henkemeyer et al., 2003; Moeller et al., 2006; Segura et al., 2007). The trans-synaptic Eph/ephrin-B interactions can result in bidirectional signaling, activating forward signaling in the Eph-expressing cell and reverse signaling in the ephrin-expressing cell (Bush and Soriano, 2009; Sloniowski and Ethell, 2012; Xu and Henkemeyer, 2012) that can promote postsynaptic spine formation and maturation during development (Henderson et al., 2001; Henkemeyer et al., 2003; Kayser et al., 2006). EphB receptors are known to directly interact with NMDARs and are important for the recruitment and retention of NMDARs at the synaptic site and modulating their function (Dalva et al., 2000; Henderson et al., 2001; Kayser et al., 2006; Nolt et al., 2011). EphB/ephrinB signaling can also influence synapse formation and maturation by regulating AMPARs at post-synaptic sites (Kayser et al., 2006; Hussain et al., 2015).

Our previous study suggests that the changes in ephrin-B1 levels in astrocytes may influence trans-synaptic interactions between neuronal ephrin-B and its EphB receptors, affecting synapse maintenance in the adult hippocampus (Koeppen et al., 2018). The goal of this study was to determine if knock-out (KO) or overexpression (OE) of astrocytic ephrin-B1 would affect synapse formation and maturation in the developing hippocampus. Ephrin-B1 KO and OE were accomplished in astrocytes during postnatal day (P) 14-28 developmental period of hippocampal synaptogenesis. Activity of CA1 hippocampal neurons was measured using both extracellular field recordings and whole-cell patch clamp electrophysiology to determine excitatory and inhibitory synaptic changes. To evaluate E/I circuit changes, we further analyzed dendritic spine density and morphology, and the density of excitatory and inhibitory synapses by immunohistochemistry through the analysis of vGlut1/PSD95, vGlut1/PV and VGAT/gephyrin-positive puncta. To examine the functional significance of the synaptic changes in ephrin-B1 KO

mice, mouse behaviors, such as sociability, social novelty, anxiety and hyperactivity were also evaluated. We observed enhanced excitation of CA1 pyramidal neurons in the developing hippocampus of astrocyte-specific ephrin-B1 KO mice. Based on our new finding, we propose new role of astrocytic ephrin-B1 in the development of both excitatory and inhibitory circuits in CA1 hippocampus during P14-P28 period. The dysregulation of E/I balance induced by astrocyte-specific deletion of ephrin-B1 in the developing hippocampus is most likely responsible for impaired sociability observed in these mice.

## Materials and Methods

### *Ethics Statement*

All mouse studies were done according to NIH and Institutional Animal Care and Use Committee at the University of California Riverside (approval number 20190015 and 20190029) guidelines; animal welfare assurance number A3439-01 is on file with the Office of Laboratory Animal Welfare (OLAW). Mice were maintained in an AAALAC accredited facility under 12-h light/dark cycle and fed standard mouse chow.

### *Mice*

To achieve specific ephrin-B1 deletion in astrocytes three different mouse lines were generated. In group 1, ERT2-Cre$^{GFAP}$ (B6.Cg-Tg(*GFAP*-cre/ERT2)505Fmv/J RRID: IMSR_JAX:012849) male mice were crossed with *ephrin-B1*$^{flox/+}$ (129S-*Efnb1* $^{flox/+}$/J, RRID: IMSR_JAX:007664) female mice to obtain either ERT2-Cre$^{GFAP}$*ephrin-B1*$^{flox/y}$ knock-out (KO) or ERT2-Cre$^{GFAP}$ control male mice. In group 2, ERT2-Cre$^{GFAP}$ mice were first crossed with Rosa-CAG-LSL-tdTomato reporter mice (CAG-tdTomato; RRID:IMSR_JAX:007909) to generate tdTomatoERT2-Cre$^{GFAP}$ mice. Then, tdTomatoERT2-Cre$^{GFAP}$ male mice were crossed

with *ephrin-B1*$^{flox/+}$ female mice to obtain either tdTomatoERT2-Cre$^{GFAP}$*ephrin-B1*$^{flox/y}$ KO or tdTomatoERT2-Cre$^{GFAP}$ control male mice allowing for tdTomato expression in astrocytes and analysis of ephrin-B1 levels. In group 3, ERT2-Cre$^{GFAP}$ mice were first crossed with Thy1-GFP-M mice (Tg(Thy1-EGFP)MJrs/J, RRID: IMSR_JAX:007788) to obtain Thy1-GFP-ERT2-Cre$^{GFAP}$ mice. Then, Thy1-GFP-ERT2-Cre$^{GFAP}$ male mice were crossed with *ephrin-B1*$^{flox/+}$ female mice to obtain either Thy1-GFP-ERT2-Cre$^{GFAP}$*ephrin-B1*$^{flox/y}$ KO or Thy1-GFP-ERT2-Cre$^{GFAP}$ control male mice allowing for GFP expression in excitatory pyramidal neurons for analysis of dendritic spines and synapses. Real-time PCR-based analysis of genomic DNA isolated from mouse tails was used to confirm genotypes by Transnetyx (Cordova, TN, USA).

In all groups of mice KO and their littermate control mice received tamoxifen at postnatal day (P) 14 intraperitoneally (IP; 0.5 mg in 5 mg/ml of 1:9 ethanol/sunflower seed oil solution) once a day for 5 consecutive days and analysis was performed at P28 (Fig. 1A). Group 1 was used for electrophysiology, immunohistochemistry, western blot and behavioral analysis; group 2 was used for immunohistochemical analysis of ephrin-B1 expression levels; and group 3 was utilized for dendritic spine and synapse analysis. To confirm specific ablation of ephrin-B1 in astrocytes ephrin-B1 immunoreactivity was analyzed in the CA1 hippocampus (Fig. 1B) of mouse group 1 (ERT2-Cre$^{GFAP}$*ephrin-B1*$^{flox/y}$ KO and their control littermates) and group 2 (tdTomatoERT2-Cre$^{GFAP}$*ephrin-B1*$^{flox/y}$ KO; Fig. 1C-D). Ephrin-B1 immunoreactivity was significantly reduced in hippocampal astrocytes of tamoxifen-treated KO mice (Fig. 1E).

To achieve overexpression (OE) of ephrin-B1 in hippocampal astrocytes we used adeno-associated viral particles (VP) containing ephrin-B1 cDNA under GFAP promoter to ensure specific expression of ephrin-B1 in astrocytes (AAV7.GfaABC1D.ephrin-B1.SV40), which is referenced in the text as AAV-ephrin-B1. Control AAV-tdTomato VP contained tdTomato

cDNA under the same GFAP promoter (AAV7.GfaABC1D.tdTomato.SV40). Experimental AAV-ephrin-B1 VP (final concentration 7.56 X $10^{12}$ viral particles/ml) and control AAV-tdTomato VP (final concentration 4.46 X $10^{12}$ viral particles/ml) were both obtained from UPenn Vector Core, http://www.med.upenn.edu/gtp/vectorcore) and processed as previously described (Koeppen et al., 2018) with modifications. Viral particles (VP) were concentrated with Amicon ultra-0.5 centrifugal filter (UFC505024, Sigma-Aldrich), which was pretreated with 0.1% Pluronic F-68 non-ionic surfactant (24040032, Thermo Fisher). Mice were anesthetized with IP injections of ketamine/xylazine mix (80 mg/kg ketamine and 10 mg/kg xylazine). To ensure for adequate anesthesia, paw pad pinch test, respiratory rhythm, righting reflex, and/or loss of corneal reflex were assessed. P14 old B6/C57 mice (RRID: IMSR_JAX: 000664) received craniotomies (1 mm in diameter) and VPs were stereotaxic injected into the dorsal hippocampus (1.8 mm posterior to bregma, 1.1 mm lateral to midline, and 1.3 mm from the pial surface; Fig. 3A). Control mice received a single injection of 1 µl of 1.16 X $10^{13}$ VP/ml AAV-tdTomato, and experimental animals received a single injection of 1 µl of 3.78 X $10^{13}$ VP/ml AAV-ephrin-B1. Post-surgery, mice received 0.3 ml of buprenorphine by subcutaneous injection every 8 h for 48 h, as needed for pain. Animals were allowed to recover for 14 days prior to analysis. P28 old mice were subjected to immunohistochemistry and whole-cell electrophysiology experiments. There was a significant increase in ephrin-B1 immunoreactivity in CA1 hippocampus on the injected ipsilateral side (OE) as compared to non-injected contralateral control side (Fig. 3B-D).

*Immunohistochemistry*

Immunohistochemistry procedures were performed as described previously (Koeppen et al., 2018). Briefly, animals were anesthetized with isoflurane and transcardially perfused with 0.9%

NaCl followed by fixation with 4% paraformaldehyde in 0.1 M phosphate-buffered saline (PBS), pH 7.4. Brains were post-fixed overnight with 4% paraformaldehyde in 0.1 M PBS and 100 μm coronal brain sections were obtained with a vibratome. Excitatory presynaptic boutons were labeled by immunostaining against vesicular glutamate transporter 1 (vGlut1) using rabbit anti-vGlut1 antibody (0.25 mg/ml, Invitrogen 482400, RRID: AB_2533843), and excitatory postsynaptic sites were identified with mouse anti-postsynaptic density-95 (PSD95) antibody (1.65 μg/ml, Invitrogen MA1-045, RRID: AB_325399). PV-positive cells were identified with mouse anti-PV antibody (2 μg/ml, Sigma-Aldrich P3088, RRID: AB 477329). Inhibitory pre-synaptic sites were detected by immunolabeling against vesicular GABA transporter (vGAT) using rabbit anti-vGAT antibody (1:100, Synaptic Systems 131002, RRID: AB_887871). Inhibitory post-synaptic sites were detected by immunolabeling against gephyrin using mouse anti-gephyrin antibody (1:500, Synaptic Systems 147111, RRID: AB_887719). Astrocytes were identified by immunolabeling against glial fibrillary acidic protein (GFAP) using mouse anti-GFAP antibody (1:500, Sigma-Aldrich G3893, RRID: AB_477010), and ephrin-B1 immunoreactivity was detected by immunostaining with goat anti-ephrin-B1 antibody (20 μg/ml, R&D Systems AF473, RRID: AB_2293419). Secondary antibodies used were Alexa Fluor 488-conjugated donkey anti-goat IgG (4 mg/ml, Molecular Probes A-11055, RRID: AB_2534102), Alexa Fluor 488-conjugated donkey anti-rabbit IgG (4mg/ml, Molecular Probes A-21206, RRID: AB_141708), Alexa Fluor 594-conjugated donkey anti-mouse IgG (4 mg/ml, Molecular Probes A-21203, RRID: AB_141633), Alexa Fluor 594-conjugated donkey anti-rabbit IgG (4 mg/ml, Molecular Probes AB150076, RRID: AB_141708), and Alexa Fluor 647-conjugated donkey anti-mouse IgG (4 mg/ml, Molecular Probes, RRID: AB). Sections were mounted on slides with

Vectashield mounting medium containing DAPI (Vector Laboratories Inc. Cat# H-1200, RRID: AB_2336790).

*Confocal Imaging and Analysis*

Confocal images of coronal brain slices containing Stratum Oriens (SO), Stratum Pyramidale (SP), Stratum Radiatum (SR) and Stratum Lacunosum-Moleculare (SLM) layers in the CA1 hippocampus were taken with a Leica SP5 confocal laser-scanning microscope as previously described (Koeppen et al., 2018). Briefly, high-resolution optical sections (1,024 x 1,024-pixel format) were captured with a 40x water-immersion and 1x zoom at 1-µm step intervals to assess ephrin-B1 immunoreactivity. Confocal images of dendritic spines and synaptic puncta were taken using a 63x objective (1.2 NA), and 1x zoom at high resolution (1,024 x 1,024-pixel format) with a 0.5-µm intervals. All images were acquired under identical conditions and processed for analysis as follows: (1) For analysis of overall ephrin-B1 immunoreactivity SO, SP and SR layers of the CA1 hippocampus were analyzed per each brain slice from at least three animals per group. Each z-stack was collapsed into a single image by projection, converted to a tiff file, encoded for blind analysis, and analyzed using Image J Software (RRID: nif-0000-30467). Each image was threshold-adjusted using default auto-threshold and then converted into a binary image. Selection tool was used to outline SO, SP and SR layers of CA1 hippocampus based on DAPI stain, saved in the ROI manager and used to measure integrated density, area and the mean intensity. (2) For analysis of ephrin-B1 immunoreactivity in astrocytes, astrocytes were visualized with tdTomato and GFAP immunoreactivity. Cell areas were outlined using selection tool, then cell area, integrated fluorescent intensity and mean intensity were measured for each astrocyte (100–200 astrocytes, z-stacks of at least 10 optical images, three mice per group, 2-3

brain slices per mouse). (3) For analysis of ephrin-B1 immunoreactivity in CA1 neurons cell bodies in SP and their proximal dendrites in SR were randomly selected and outlined using selection tool. These regions of interest were saved in the ROI manager and used to measure area and perform analysis of integrated fluorescent intensity and mean intensity. (4) For the analysis of vGlut1, PSD95, and PV immunolabeling, each image in the series was threshold-adjusted to identical levels (0-160 intensity) and puncta numbers (0.5-10 $\mu m^2$) were collected using ImageJ software. Three adjacent areas from SR and SLM were analyzed per each hippocampus from four animals per group. (5) For the analysis of gephyrin and vGAT immunoreactive puncta cell bodies and dendrites of GFP-expressing CA1 neurons were randomly selected for the analysis. Each z-stack was collapsed into a single image by projection, converted to a tiff file, encoded for blind analysis and analyzed using Image J Software (RRID: nif-0000-30467). Each image was threshold-adjusted using default autothreshold and then converted into a binary image. The watershed function was applied to each image in order to separate overlapping puncta. A selection tool was used to define regions of interest (ROI) around CA1 neuronal cell bodies in SP, primary and secondary dendrites in SR, and dendrites in SO layers. These regions of interest were saved in the ROI manager and used to measure area and to perform puncta (0.5-10 $\mu m^2$) analysis using particle analysis tool. Colocalization of vGlut1/PSD95, vGlut1/PV, gephyrin/vGAT was analyzed using ImageJ plugin for colocalization (https://imagej.nih.gov/ij/plugins/colocalization.html), Statistical analysis was performed with two-way ANOVA followed by Tukey post-hoc analysis or unpaired t-test using GraphPad Prism 7 software (RRID: SCR_002798), data represent mean ± standard error of the mean (SEM).

*Dendritic Spine Analysis*

Dendritic spines were identified with GFP in Thy1-GFP-ERT2-Cre$^{GFAP}$*ephrin-B1*$^{flox/y}$ (KO) or Thy1-GFP-ERT2-Cre$^{GFAP}$ (Control) male mice (group 3) expressing GFP in hippocampal pyramidal neurons as previously described (Koeppen et al., 2018). Briefly, animals were anesthetized with isoflurane and transcardially perfused initially with 0.9% NaCl, followed by fixation with 4% PFA in 0.1 M PBS, pH 7.4. Brains were post-fixed for 2 h in 4% PFA in 0.1 M PBS, and 100 µm coronal sections were obtained with a vibratome. CA1 hippocampal neurons were imaged using Leica SP5 confocal microscope. 5 GFP-expressing neurons were randomly selected per animal, and dendrites were imaged using a 63x-oil immersion objective (1.2 NA) and 1x zoom. Three-dimensional fluorescent images were created by the projection of each z-stack containing 50 high-resolution optical serial sections (1,024 x 1,024-pixel format) taken at 0.5-µm intervals in the X-Y plane. Quantifications of the spine density (spines per 10 µm dendrite), lengths (µm) and volumes (µm$^3$) were carried out using Neurolucida 360 software (MicroBrightField RRID: SCR_001775). Statistical analysis was performed with two-way ANOVA followed by Tukey's post hoc test analysis using GraphPad Prism 7 software (GraphPad Prism, RRID: SCR_002798), data represent mean ± SEM.

*Synaptosome Isolation and Western Blot Analysis*

Isolation of hippocampal synaptosomes was performed as previously described with modifications (Hollingsworth et al., 1985; Koeppen et al., 2018). Briefly, hippocampal tissues from P28 old control or KO mice (group 1) were homogenized in 1 ml synaptosome buffer (in mM: 124 NaCl, 3.2 KCl, 1.06 $KH_2PO_4$, 26 $NaHCO_3$, 1.3 $MgCl_2$, 2.5 $CaCl_2$, 10 Glucose, 20 HEPES). Homogenates were first filtered through a 100 µm nylon net filter (NY1H02500, Millipore) and then through a 5 µm nylon syringe filter (SF15156, Tisch International).

Homogenate flow through was collected and synaptosomes were spun down at 10,000 g, 4°C, for 30 min. Synaptosomes were resuspended in 800 µl synaptosome buffer. To confirm synaptosome enrichment, levels of synapsin-1 and PSD95 were analyzed in tissue homogenates and synaptosome fractions with western blot analysis (see extended data Fig. 4-1). Isolated hippocampal synaptosome samples were centrifuged at 10,000 g, 4°C, for 30 min, and pellets were re-suspended in lysis buffer (50 mM Tris, 100 mM NaCl, 2% TritonX-100, 10 mM EDTA) containing 2% protease inhibitor cocktail (P8340, Sigma-Aldrich) and incubated for 2 h at 4°C. Samples were added to 2X Laemmli Buffer (S3401, Sigma-Aldrich) and run on an 8-16% Tris-Glycine Gel (EC6045BOX, Invitrogen). Protein samples were transferred onto a nitrocellulose blotting membrane (10600007, GE Healthcare). Blots were blocked with 5% milk in TBS (10 mM Tris, 150 mM NaCl, pH 8.0), followed by immunostaining with mouse anti-PSD95 (1.65 µg/ml, Invitrogen MA1-045, RRID: AB_325399), rabbit anti-GluA1 (1:100, Millipore AB1504, RRID: AB_2113602), rabbit anti-GluA2/3 (0.1 µg/ml, Millipore AB1506, RRID: AB_90710), rabbit anti-synapsin-1 (0.2 µg/ml, Millipore AB1543P, RRID: AB_90757), or mouse anti-GAPDH (0.2 µg/ml, Thermo Fisher Scientific 39-8600, RRID: AB_2533438) antibodies in 0.1% tween 20/TBS at 4°C for 16 h. Secondary antibodies used were HRP conjugated donkey anti-mouse IgG (Jackson ImmunoResearch 715-035-150, RRID: AB_2340770) or HRP conjugated goat anti-rabbit IgG (Jackson ImmunoResearch 111-035-003, RRID: AB_2313567). Blots were incubated in ECL 2 Western Blotting Substrate (80196, Pierce) and a signal was collected with CL-XPosure film (34090, Pierce). Band density was analyzed by measuring band and background intensity using Adobe Photoshop CS5.1 software (RRID: SCR_014199). Statistical analysis was performed with unpaired t-test using GraphPad Prism 7 software (RRID: SCR_002798), data represent mean ± SEM.

*Extracellular Field Recordings*

P28 old mice (group 1) were used for electrophysiological experiments, two weeks after the first tamoxifen injection. Animals were deeply anesthetized with isoflurane and decapitated. The brains were rapidly removed and immersed in ice-cold artificial cerebrospinal fluid (ACSF) with high $Mg^{2+}$ and sucrose concentration containing: (in mM) 3.5 KCl, 1.25 $NaH_2PO_4$, 20 D(+)-glucose, 185 sucrose, 26 $NaHCO_3$, 10 $MgCl_2$ and 0.50 $CaCl_2$, pH of 7.4, and saturated with 95% $O_2$/5% $CO_2$. Transverse 350 µm hippocampal slices were prepared by using a vibrating blade microtome (LeicaVT1000s, Leica Microsystems; Buffalo Grove, IL, USA) in ice-cold slicing solution bubbled with 95% $O_2$/5% $CO_2$. Slices were then transferred into a holding chamber containing oxygenated ACSF (in mM: 124 NaCl, 3.5 KCl, 1.25 $NaH_2PO_4$, 10 D(+)-glucose, 26 $NaHCO_3$, 2 $MgCl_2$, and 2 $CaCl_2$, pH 7.4) and incubated for 1 h at 33°C, then kept at room temperature. For recordings, slices were transferred to a recording chamber and continuously perfused with oxygenated ACSF at a flow rate of 1 ml/min at 33˚C. Slices were equilibrated in recording chamber for 10 min to reach a stable baseline response prior to running experimental protocols. Glass microelectrodes were pulled with a Sutter P-97 micropipette puller (Sutter Instrument, Novato, CA, USA; RRID: SCR_016842) with a tip resistance of 1-3 MΩ and filled with 3 M NaCl. Glass microelectrodes were positioned in the SP and SR areas of CA1 hippocampus for extracellular recording. Synaptic responses were evoked by stimulating Schaffer collaterals (SC) using a bipolar tungsten electrode (WPI, Sarasota, FL, USA), approximately 200 µm away from the recording electrodes. Potentials were amplified (Axoclamp-2B, Molecular Devices, Sunnyvale, CA, USA), digitized at a sampling rate of 10 kHz, and analyzed offline using pClamp 10.7 software (Molecular Devices; RRID:

SCR_011323). All electrophysiological responses were digitally filtered at 1 kHz low-pass filter to improve signal-to-noise ratio.

Dendritic potentials typically consisted of a small presynaptic fiber volley (FV) followed by a negative field excitatory postsynaptic potential (fEPSP). The amplitude of the FV reflects the depolarization of the presynaptic terminals and was quantified by measuring the amplitude of first negative waveform. The fEPSP slope reflects the magnitude of the postsynaptic dendritic depolarization and was quantified by measuring the 20-80% slope of the second negative waveform. Postsynaptic neuronal firing is represented by the amplitude of the population spike (PS), which was calculated as the voltage difference between first positive peak and the most negative peak of the trace.

Input-output (I/O) curves were generated to examine basal synaptic transmission by incrementally increasing stimulation intensity, beginning at 0.10 mA and increasing stimulation by 0.10 mA until maximal somatic PS amplitude was reached. Maximal PS amplitude was regarded as maximal neuronal output. Maximal fEPSP slope and PS response along with 30-50% of maximal fEPSP slope and PS were determined.

For electrophysiological data, two-way ANOVA was used followed by Bonferroni test to evaluate the effects of astrocytic ephrin-B1 deletion on the I/O curves. In all electrophysiological recordings, the data represent mean ± SEM.

*Whole-Cell Patch Clamp Recordings*

Brain slice preparation for whole-cell patch clamp was same as above; briefly, brains were rapidly removed and immersed in ice cold “slushy” artificial cerebrospinal fluid (ACSF) with high $Mg^{2+}$ and sucrose concentration containing the following (in mM): 87 NaCl, 75 sucrose, 2.5

KCl, 0.5 $CaCl_2$, 7 $MgCl_2$, 1.25 $NaH_2PO_4$, 25 $NaHCO_3$, 10 glucose, 1.3 ascorbic, acid, 0.1 kynurenic acid, 2.0 pyruvate, and 3.5 MOPS pH of 7.4 and saturated with 95% $O_2$/5% $CO_2$. Transverse hippocampal slices (350 µm) were prepared by using a vibrating blade microtome (Campden 5100mz-Plus, Campden Instruments Ltd.) in high $Mg^{2+}$/sucrose ACSF solution bubbled with 95% $O_2$/5% $CO_2$. Slices were then incubated in a holding chamber containing oxygenated high $Mg^{2+}$/sucrose ACSF for 30 min at room temperature and then transferred into ACSF (in mM: 125 NaCl, 2.5 KCl, 2.5 CaCl2, 1.3 MgCl2, 1.25 NaH2PO4, 26 NaHCO3, 15 glucose 3.5 MOPS, pH of 7.4) for an additional 30 min at room temperature. Slices were transferred to a recording chamber and continually perfused with oxygenated ACSF at a flow rate of 1 ml/min at 33˚C.

Whole-cell patch experiments were conducted blind, as described in by Castañeda-Castellanos et al. (Castaneda-Castellanos et al., 2006). Electrical stimuli (0.1 Hz) were delivered through a bipolar, Teflon®-coated tungsten electrode (FHC, Bowdin, ME, USA) placed in the SR area of CA1 hippocampus to stimulate Schaffer collaterals, approximately 200 µm away from recording electrode, and CA1 hippocampal pyramidal neurons were voltage-clamped. Tight-seal whole-cell recordings were obtained using pipettes made from borosilicate glass capillaries pulled on a Narishige PC-10 vertical micropipette puller (Narishige, Tokyo, Japan). Pipette resistance ranged from 3 to 4 MΩ and filled with an internal solution containing: (in mM) 130 CsOH, 130 D-gluconic acid, 0.2 EGTA, 2 $MgCl_2$, 6 CsCl, 10 Hepes, 2.5 ATP-Na, 0.5 GTP-Na, 10 phosphocreatine and 0.1% Biocytin for cellular post labeling, pH adjusted to 7.2-7.3 with CsOH, osmolarity adjusted to 300-305 mOsm with ATP-Na. CA1 neurons were voltage-clamped at either -70 mV to measure AMPAR-evoked responses or +40 mV to measure NMDAR-evoked responses. Amplitudes of evoked AMPAR-mediated responses were measured at peak response

following stimulus artifact, and amplitudes of evoked NMDAR-mediated responses were measured 60 ms following stimulus artifact to isolate NMDAR-only mediated responses. 1 µM tetrodotoxin was added to isolate miniature (m) EPSC responses. All EPSCs were recorded in the presence of 50 µM picrotoxin, a $GABA_A$ receptor antagonist, to block $GABA_A$-mediated currents. To measure IPSCs, electrical stimulation was delivered in the SR region to stimulation inhibitory neurons (in close proximity, approximately 200 µm away from recording electrode) and CA1 hippocampal pyramidal neurons were voltage-clamped and recorded at 0 mV in the presence of 10 µM NBQX, an AMPAR antagonist, and 50 µM D-AP5, a NMDA receptor antagonist. EPSCs and IPSCs were recorded using an EPC-9 amplifier (HEKA Elektronik, Lambrecht, Germany), filtered at 1 kHz, digitized at 10 kHz, and stored on a personal computer using pClamp 10.7 software (Molecular Device) to run analysis. The series resistance was <25 MΩ and was compensated. Both series and input resistance were monitored throughout the experiment by delivering 5 mV voltage steps. If the series resistance changed more than 20% during the course of an experiment, the data was discarded. AMPAR- and NMDAR-mediated evoked EPSCs, evoked IPSCs, mEPSCs and mIPSCs were analyzed by Clampfit 10.7 software (Molecular Device) and customized Matlab script. Miniature events with the amplitude of 5pA or higher were included in the analysis. To test the effects of ephrin-B1 KO in astrocytes, group 1 KO male mice and their control littermates were used. To test the effects of ephrin-B1 overexpression, recordings from AAV-ephrin-B1 injected ipsilateral side were included in OE group. As no significant differences were observed between recordings from contralateral non-injected side and AAV-tdTomato injected hippocampi, both were combined in the control group. All averaged data were presented as means ± SEM. Statistical significance was determined by unpaired Student's *t*-test using Prism 7 software (Graph Pad Software, Avenida, CA).

*Social Novelty Test*

Sociability and social memory were studied in KO male mice and their control littermates (group 1) using a three-chamber test as described previously (Kaidanovich-Beilin et al., 2011). Briefly, a rectangular box contained three adjacent chambers 19 x 45 cm each, with 30 cm high walls and a bottom constructed from clear plexiglass. The three-chambers were separated by dividing walls, which were made from clear plexiglass with openings between the middle chamber and each side chamber. Removable doors over these openings permitted chamber isolation or free access to all chambers. All testing was done in a brightly lit room (650 lux), between 9 am and 2 pm. Prior to testing, mice were housed in a room with a 12-h light/dark cycle with *ad libitum* access to food and water. The cages were transferred to the behavioral room 30 min before the first trial began for habituation. The test mouse was placed in the central chamber with no access to the left and right chambers and allowed to habituate to the test chamber for 5 min before testing began. Session 1 measured sociability; in session 1, another mouse (stranger 1) was placed in a wire cup-like container in one of the side chambers. The opposite side had an empty cup of the same design. The doors between the chambers were removed and the test mouse was allowed to explore all three chambers freely for 10 min, while being digitally recorded from above. The following parameters were monitored: the duration of direct contact between the test mouse and either the stranger mouse or empty cup and the duration of time spent in each chamber. Session 2 measured social memory; in session 2, a new mouse (stranger 2) was placed in the empty wire cup in the second side chamber. Stranger 1, a now familiar mouse, remained in the first side chamber. The test mouse was allowed to freely explore all three chambers for another 10 min, while being recorded, and the same parameters were monitored. Placement of

stranger 1 in the left or right side of the chamber was randomly altered between trials. The floor of the chamber was cleaned with 2-3% acetic acid, 70% ethanol, and water between tests to eliminate odor trails. Assessments of the digital recordings were done using TopScan Lite software (Clever Sys. Inc, Reston, VA 20190). To measure changes in social preference and social memory, percent time spent in each chamber was calculated in each test. Further, a social preference index ($\frac{time\ in\ S1\ chamber}{time\ in\ S1\ chamber + time\ in\ empty\ chamber}$) and social novelty index ($\frac{time\ in\ S2\ chamber}{time\ in\ S2\ chamber + time\ in\ S1\ chamber}$) were calculated as described previously (Nygaard et al., 2019). For social preference index, values <0.5 indicate more time spent in the empty chamber, >0.5 indicate more time spent in the chamber containing stranger 1, and 0.5 indicates equal amount of time in both chambers. For social novelty index, values <0.5 indicate more time spent in the chamber containing stranger 1 or now familiar mouse, >0.5 indicate more time spent in the chamber containing stranger 2 or new stranger mouse, and 0.5 indicates equal amount of time in both chambers. Statistical analysis was performed using two-way ANOVA followed by Tukey's post hoc test.

*Open Field Behavior Test*

Locomotor activity and anxiety was evaluated using a standard open field exploration test as previously described with modifications (Lovelace et al., 2020). The apparatus consisted of a 42.5 × 30 cm open field arena with 30 cm-high walls constructed from opaque acrylic sheets and a clear acrylic sheet for the bottom with a grid placed underneath it for scoring purposes. All testing was done in a brightly lit room (650 lux), between 9 am and 2 pm. Prior to testing mice were housed in a room with a 12-h light/dark cycle with *ad libitum* access to food and water. Mice were initially habituated to the testing room for at least 30 min before testing. During

testing, animals were allowed to freely explore the open field for 10 min. The floor of the chamber was cleaned with 2-3% acetic acid, 70% ethanol, and water between tests to eliminate odor trails. Assessments of the digital recordings were done by blinded observers using TopScan Lite software (Clever Sys. Inc, Reston, VA 20190). A tendency to travel to the center and percent time spent in thigmotaxis was used as an indicator of anxiety (Yan et al., 2004; Yan et al., 2005). Average velocity and total line crosses were measured to score locomotor activity. Statistical analysis was performed using Student's *t*-test.

**Results**

In the current study, we examined whether deletion or overexpression of ephrin-B1 in astrocytes during a developmental critical period affects the formation and maturation of synapses in the hippocampus. First, we evaluated excitatory and inhibitory synaptic changes using both extracellular field recordings and whole-cell patch clamp electrophysiology. Next, we assessed the number of dendritic spines and synapses on CA1 hippocampal neurons using immunohistochemistry. Finally, social behaviors, anxiety and hyperactivity were evaluated in ephrin-B1 KO mice to examine functional significance of the astrocyte-specific deletion of ephrin-B1 during postnatal brain development.

**Ephrin-B1 loss in developing astrocytes enhances excitability of CA1 hippocampal neurons.**

Previously we have shown that astrocytic ephrin-B1 is involved in the maintenance of excitatory but not inhibitory synapses in the adult hippocampus (Koeppen et al., 2018; Nguyen et al., 2020). Ephrins and Eph receptors are identified as risk genes for the development of ASD in humans (Sanders et al., 2012). Mouse models of ASD are also shown to have altered E/I balance

as a result of aberrant excitatory and inhibitory synapse development and plasticity, inhibitory neuron development, neuronal excitability, and glial cell dysfunction (Lee et al., 2017). Therefore, we assessed the effects astrocyte-specific deletion or overexpression of ephrin-B1 in developing hippocampus during the critical developmental period when maturation of neuronal circuits occurs.

To achieve specific ephrin-B1 deletion in astrocytes ERT2-Cre$^{GFAP}$*ephrin-B1*$^{flox/y}$ KO mice (group 1) were generated and ERT2-Cre$^{GFAP}$ mice were used as a control (Fig. 1A). To allow for tdTomato expression in astrocytes in order to analysis of ephrin-B1 levels in astrocytes tdTomatoERT2-Cre$^{GFAP}$*ephrin-B1*$^{flox/y}$ KO mice (group 2) were generated and tdTomatoERT2-Cre$^{GFAP}$ mice were used as controls (Fig. 1A). To achieve GFP expression in excitatory pyramidal neurons for analysis of dendritic spines and synapses Thy1-GFP-ERT2-Cre$^{GFAP}$*ephrin-B1*$^{flox/y}$ KO (group 3) and their corresponding Thy1-GFP-ERT2-Cre$^{GFAP}$ control mice were generated (Fig. 1A). In all groups of mice KO and their littermate control mice received tamoxifen at P14 intraperitoneally (IP; 0.5 mg in 5 mg/ml of 1:9 ethanol/sunflower seed oil solution) once a day for 5 consecutive days and analysis was performed at P28 (Fig. 1A). To confirm specific ablation of ephrin-B1 in astrocytes, ephrin-B1 immunoreactivity was analyzed in the CA1 hippocampus (Fig. 1B) of mouse group 1 (ERT2-Cre$^{GFAP}$*ephrin-B1*$^{flox/y}$ KO and their control littermates) and group 2 (tdTomatoERT2-Cre$^{GFAP}$*ephrin-B1*$^{flox/y}$ KO and their control littermates; Fig. 1C-D). Ephrin-B1 immunoreactivity was significantly reduced in hippocampal astrocytes of KO as compared to control mice (Fig. 1C-E; extended data Fig. 1-1, t-test; $t_{(16)} = 2.908$ $p < 0.0103$). We also observed changes in the distribution of ephrin-B1 immunoreactivity in CA1 neurons of KO mice (Fig. 1C-D) with a significant reduction in cell bodies (Fig. 1E; C:

extended data Fig. 1-1; t-test, $t_{(18)}$=5.538 $p < 0.0001$) and an increase in proximal dendrites as compared to control mice (Fig. 1E; extended data Fig. 1-1; t-test, $t_{(31)}$=5.326 $p < 0.0001$).

To determine if loss of astrocytic ephrin-B1 alters neuronal activity in the developing hippocampus, acute hippocampal slices were prepared for extracellular field recordings from group 1 KO male mice and their control counterparts at P28. Presynaptic FV amplitude, postsynaptic fEPSP slope, and somatic PS amplitude of neuronal responses were recorded in SR and SP layers of CA1 hippocampus and input-output (I/O) curves were generated by incrementally increasing stimulation intensity of SC in CA3 hippocampus (Fig. 1F-H). Extracellular field recordings revealed that the loss of astrocytic ephrin-B1 increased the excitability of CA1 hippocampal neurons. Both, FV response amplitude (Fig. 1F; extended data Fig. 1-2, 1-3; two-way ANOVA; stimulation intensity $F_{(14, 540)} = 89.41$; genotype $F_{(1, 540)} = 8.064$, $p = 0.0047$, $p < 0.0001$) and fEPSP slope were significantly higher in KO mice (Fig. 1G; extended data Fig. 1-2, 1-3; two-way ANOVA; stimulation intensity $F_{(14, 386)} = 41.58$, $p < 0.0001$ ; genotype $F_{(1, 386)} = 39.26$, $p < 0.0001$). PS response amplitude was also greatly enhanced in KO mice (Fig. 1H; extended data Fig. 1-2, 1-3; two-way ANOVA; stimulation intensity $F_{(14, 510)} = 42.41$, $p < 0.0001$; genotype $F_{(1, 510)} = 64.18$, $p < 0.0001$).

These results demonstrate that hippocampal CA1 pyramidal neurons show enhanced excitability following astrocyte specific deletion of ephrin-B1 during early postnatal development, suggesting an alteration in E/I balance.

**Enhanced evoked excitatory postsynaptic AMPAR and NMDAR-mediated responses and higher mEPSC amplitude are detected in CA1 neurons of astrocyte-specific ephrin-B1 KO mice.**

To determine the mechanism of enhanced hippocampal activity in astrocyte-specific ephrin-B1 KO mice, whole-cell voltage clamp electrophysiology was used to measure spontaneous and evoked excitatory responses from CA1 pyramidal neurons of P28 old control and KO mice in the presence of $GABA_A$ receptor antagonist picrotoxin (Fig. 2). I/O curves were generated (not shown) and stimulation that induced maximum response was used to measure AMPAR- and NMDAR-mediated EPSCs. We observed a significant increase in both AMPAR- and NMDAR-mediated EPSCs in KO mice compared to control (Fig. 2C; extended data Fig. 2-1; AMPAR: t-test, $t_{(16)} = 2.393$, $p = 0.0293$; NMDAR: t-test, $t_{(19)} = 4.10$, $p = 0.0006$). Interestingly, AMPAR/NMDAR ratio was not significantly different between control and KO mice (Fig. 2D; extended data Fig. 2-1; $t_{(16)} = 1.297$, $p = 0.2130$). There were also no differences in mEPSC frequencies between control and KO mice (Fig. 2F-G; extended data Fig. 2-1; t-test, $t_{(9)} = 1.259$,$p = 0.2398$). In contrast, we observed a significant shift in cumulative probability distribution of mEPSC amplitude to a higher amplitude (Fig. 2H; K–S test, n = 190 and 160 for control and KO group, respectively, $p < 0.0001$, $D = 0.3119$) and increased mEPSC average amplitude (Fig. 2I; extended data Fig. 2-1; t-test, $t_{(9)} = 2.208$, $p = 0.0273$). Our results suggest enhanced postsynaptic excitatory responses in CA1 neurons following astrocyte-specific deletion of ephrin-B1 during P14-P28 developmental period.

**Overexpression of astrocytic ephrin-B1 in hippocampus CA1 affects AMPAR- and NMDAR-mediated responses and mEPSC amplitude.**

Next, we examined the effects of the overexpression of ephrin-B1 in hippocampal astrocytes during P14-P28 period on excitatory activity in CA1 pyramidal neurons. To achieve overexpression (OE) of ephrin-B1 or control (C) tdTomato in hippocampal astrocytes we used

viral particles (VP) containing ephrin-B1 cDNA (AAV-ephrin-B1) or tdTomato cDNA (AAV-tdTomato). VPs were stereotaxic injected into the dorsal hippocampus (Fig. 3A). Control P14 old male mice were unilaterally injected with AAV-tdTomato (1.16 X $10^{10}$ VP), and experimental animals with AAV-ephrin-B1 (3.78 X $10^{10}$ VP). At P28, mice were subjected to immunohistochemistry and whole-cell electrophysiology experiments. There was a significant increase in ephrin-B1 immunoreactivity in all three layers of CA1 hippocampus on the AAV-ephrinB1 injected side (ipsilateral side, OE) as compared to control non-injected (contralateral side, Fig. 3B-D; extended data Fig. 3-1; SO: t-test, $t_{(21)}$=5.366, $p < 0.0001$; SP: t-test, $t_{(21)}$=6.220, $p< 0.0001$; SR: t-test, $t_{(21)}$=4.062, $p= 0.0006$).

For whole-cell voltage clamp electrophysiology, I/O curves were generated and stimulation that induced the maximum response was used to measure AMPAR- and NMDAR-mediated EPSCs. We noted higher amplitude of evoked AMPAR- and NMDAR-mediated responses in control slices from AAV-tdTomato injected mice (control group for OE mice; Fig. 3E,F) compared to control slices from ERT2-Cre$^{GFAP}$ mouse line (control group for KO mice; Fig. 2B,C), potentially due to the effects of viral injection or the differences between mouse lines. Therefore, comparisons were made only between AAV-injected OE group and corresponding control group. Recordings from AAV-ephrin-B1 injected ipsilateral side were included in OE group (Fig. 3A). No significant differences were observed between recordings from contralateral non-injected side of AAV-ephrin-B1 injected mice and ipsilateral side of AAV-tdTomato injected mice, both were combined in the control group (Fig. 3A). A significant reduction of evoked AMPAR- and NMDAR-mediated responses was observed in the OE group compared to control (Fig. 3E, F; extended data Fig. 3-2; AMPAR: t-test, $t_{(23)} = 2.692$, $p = 0.0130$; NMDAR: t-test, $t_{(20)} = 3.573$, $p = 0.0019$), with no effect to AMPAR/NMDAR EPSC

ratio (Fig. 3G; extended data Fig. 3-2; t-test, $t_{(20)} = 0.9733$, $p = 0.3426$). However, mEPSC were unchanged in the OE group compared to control (Fig. 3H), including cumulative probability of inter-event interval (Fig. 3H, I; K–S test, n = 550 and 360 for control and OE group, respectively, $p = 0.4819$, $D = 0.1408$) and average frequency of mEPSCs (Fig. 3J; extended data Fig. 3-2; t-test, $t_{(12)} = 1.036$, $p = 0.3206$). In contrast, the OE group exhibited a significant leftward shift in cumulative probability of mEPSC amplitude, showing a reduced number of larger events with >10pA amplitude, (Fig. 3K; K–S test, n = 550 and 360 for control and OE group, respectively, $p = 0.0145$, $D = 0.1065$) and a reduced average mEPSC amplitude compared to their control counterparts (Fig. 3L; extended data Fig. 3-2; t-test, $t_{(12)} = 1.821$, $p = 0.0468$). In the OE group, the reduced number of the events with large amplitude may potentially indicate a reduced strength or loss of synapses at the soma or proximal dendrites of CA1 hippocampal neurons, in a close proximity to recording electrode.

Together this further confirms that astrocytic ephrin-B1 negatively affects excitatory synaptic transmission in the developing hippocampus, such that the loss of ephrin-B1 in astrocytes enhances, but its overexpression reduces excitatory responses in CA1 hippocampal neurons.

**Excessive excitatory synapse formation is observed in CA1 hippocampus of developing KO mice.**

Next, we examined whether loss of ephrin-B1 from astrocytes would also affect the number of excitatory synapses in CA1 hippocampus by co-immunostaining against presynaptic vGlut1 and postsynaptic PSD95 using brain slices from group 1 KO and their control mice (Fig. 4A, B). We observed a significant increase in vGlut1-positive puncta (Fig. 4C; extended data

Fig. 4-1; t-test, $t_{(21)} = 4.238$, $p = 0.0004$), PSD95-positive puncta (Fig. 4D; extended data Fig. 4-1; t-test, $t_{(17)} = 2.801$, $p = 0.0123$) and vGlut1/PSD95 co-localization (Fig. 4E; extended data Fig. 4-1; t-test, $t_{(51)} = 3.784$, $p = 0.0004$) in the SR but not SLM layer of CA1 hippocampus of KO mice compared to control mice. Further, dendritic spine density was significantly higher in KO compared to control (Fig. 4G; extended data Fig. 4-2; t-test, $t_{(31)} = 2.78$, $p = 0.0092$). Together, our results suggest that the loss of astrocytic ephrin-B1 results in excessive excitatory synapse formation on excitatory CA1 neurons, which may contribute to enhanced excitability.

**Developmental astrocyte-specific deletion of ephrin-B1 affected size of dendritic spines but not synaptic levels of AMPARs.**

To assess synapse maturation, spine morphology was assessed using group 3 mice. Dendritic spines were identified with GFP in Thy1-GFP-ERT2-Cre$^{GFAP}$*ephrin-B1*$^{flox/y}$ (KO) or Thy1-GFP-ERT2-Cre$^{GFAP}$ (Control) male mice expressing GFP in hippocampal pyramidal neurons (Fig. 4F). Spine length was comparable between control and KO mice (Fig. 4H; extended data Fig. 4-2; t-test, $t_{(31)} = 0.0697$, $p = 0.9449$). Interestingly, KO mice had a greater proportion of spines with smaller heads (0-0.5 $um^3$; extended data Fig. 4-3; two-way ANOVA, Tukey's post hoc test, $p < 0.0001$) and a smaller percent of medium size spines (0.5-1.0 $um^3$; Fig. 4I; extended data Fig. 4-3; two-way ANOVA, Tukey's post hoc test, $p = 0.0162$) but similar levels of large, more mature spines (>1.0 $um^3$; Fig. 4I; extended data Fig. 4-3; two-way ANOVA, Tukey's post hoc test, $p = 0.9617$) compared to control animals.

In addition, the levels of synaptic AMPAR subunits GluA1 and GluA2/3 were analyzed in developing hippocampus of control and KO mice. Crude synaptosomes were isolated from P28 hippocampi of control and KO mice (group 1) and analyzed with immunoblotting (Fig. 4K).

Significant enrichment of PSD-95 and synapsin1 in synaptosome fraction compared to lysates was also confirmed by immunoblotting (extended data Fig. 4-4). Synaptic PSD95 levels (Fig. 4K; extended data Fig. 4-5, t-test, $t_{(10)} = 0.9338$, $p = 0.3724$) and levels of AMPAR subunits GluA1 (Fig. 4K; extended data Fig. 4-5, t-test, $t_{(10)} = 1.085$, $p = 0.3036$) and GluA2/3 (Fig. 4K; extended data Fig. 4-5, t-test, $t_{(10)} = 0.1792$, $p = 0.8613$) were not significantly different between control and KO mice. These results are consistent with similar AMPAR/NMDAR EPSC ratio that was observed in control and KO mice (Fig. 2D), suggesting no differences in the functional maturation of excitatory synapses between control and KO mice.

Despite no effect on functional maturation of excitatory synapses, KO mice exhibited a larger proportion of dendritic spines with smaller heads, suggesting changes in structural maturation.

**Inhibitory postsynaptic currents are reduced in CA1 neurons of astrocytic ephrin-B1 KO mice, while overexpression enhances evoked IPSCs in CA1 hippocampus.**

To determine if astrocytic ephrin-B1 affects inhibitory synapses, inhibitory post-synaptic currents (IPSCs) were recorded from CA1 hippocampal neurons in brain slices from group 1 KO and their control mice using whole-cell voltage clamp electrophysiology (Fig. 5A). In the presence of NMDAR and AMPAR blockers, D-AP5 and NBQX, we observed a significant decrease in evoked IPSC amplitude in CA1 hippocampal neurons of KO mice compared to control (Fig. 5B; extended data Fig. 5-1; t-test, $t_{(20)} = 1.90$, $p = 0.0360$). However, the cumulative probability of inter-event interval (Fig. 5D; K–S test, n = 3500 and 4500 for control and KO group, respectively, $p = 0.1765$, $D = 0.9539$) and average frequency of mIPSC were unchanged in KO group compared to control (Fig. 5E; extended data Fig. 5-1; t-test, $t_{(13)} = 0.02485$, $p =$

0.9806). KO mice exhibited a significant leftward shift of cumulative probability of mIPSC amplitude (Fig. 5F; K–S test, n = 3500 and 4500 for control and KO group, respectively, p = 0 < 0.0001, D = 0.0541) and a reduced average mEPSC amplitude compared to their control counterparts (Fig. 5G; extended data Fig. 5-1; t-test, $t_{(13)}$ = 0.7904, p = 0.04435). Reduced proportion of high-amplitude (>10pA) events in the KO group may suggest a reduced strength or loss of inhibitory synapses on the cell body or proximal dendrites of CA1 hippocampal neurons (in a close proximity to the recording electrode).

Conversely, to determine if the overexpression of astrocytic ephrin-B1 affects inhibitory synapses, IPSCs were recorded from CA1 hippocampal neurons on AAV-ephrin-B1 injected ipsilateral side (OE, Fig. 3A) using whole-cell voltage clamp electrophysiology (Fig. 5H-N). Control group included recordings from both contralateral non-injected side of AAV-ephrin-B1 injected mice and ipsilateral side of AAV-tdTomato injected mice (Fig. 3A), as there were no significant differences observed between these groups. Interestingly, we observed a significant increase in evoked IPSC amplitude in CA1 hippocampal neurons of the OE group compared to control (Fig. 5I; extended data Fig. 5-2; t-test, $t_{(19)}$; = 2.135 p = 0.0230). The cumulative probability of inter-event interval exhibited a rightward shift in OE mice (Fig. 5K; K–S test, n = 4800 and 4100 for C and OE group, respectively, p = 0<0.0001, D = 0.1018); however, the average frequency of mIPSCs was unchanged in the OE group compared to control (Fig. 5L; extended data Fig. 5-2; t-test, $t_{(24)}$ = 1.32, p = 0.1988). The cumulative probability of mIPSC amplitude (Fig. 5M; K–S test, n = 4800 and 4100 for control and OE group, respectively, p > 0.9999, D = 1.000) and average mEPSC amplitude were similar between the OE and control groups (Fig. 5N; extended data Fig. 5-2; t-test, $t_{(24)}$ = 0.39, p = 0.6999).

Our results show that loss of ephrin-B1 from astrocytes during P14-P28 developmental period leads to reduced evoked IPSCs and mIPSC amplitude in CA1 hippocampal neurons, but overexpression of ephrin-B1 in astrocytes resulted in enhanced evoked IPSCs without affecting mIPSC amplitude.

**Changes in the density of PV-positive inhibitory neurons in CA1 hippocampus may contribute to impaired inhibition in KO mice.**

To determine if astrocyte-specific deletion of ephrin-B1 affects the inhibitory drive onto CA1 hippocampal neurons, inhibitory synaptic sites were detected on GFP-expressing dendrites of CA1 excitatory neurons with immunostaining against VGAT and gephyrin in brain slices from group 3 KO male mice and their controls (Fig. 6A, B). We observed no effect of ephrin-B1 deletion from developing astrocytes on VGAT/gephyrin co-localized puncta along the first order dendrites (Fig. 6C; extended data Fig. 6-1; t-test, $t_{(51)=}$ 1.449, p= 0.1534) or second order dendrites (Fig. 6C; extended data Fig. 6-1; t-test, $t_{(22)}$= 0.7795, p=0.4440) of CA1 neurons in SR area of the hippocampus. However, we did observe a significant decrease in VGAT/Gephyrin co-localization on the cell bodies of CA1 neurons in SP area (Fig. 6D; extended data Fig. 6-1; t-test; $t_{(60)}$=2.030, p=0.0468) and the dendrites of the CA1 neurons in SO area (Fig. 6E; extended data Fig. 6-1; t-test, $t_{(18)}$=2.307, p=0.0332).

We also observed a significant two-fold decrease in the density of PV-positive (PV) inhibitory neurons in the CA1 hippocampus of KO mice compared to control mice in SO (Fig. 6G; extended data Fig. 6-2; $t_{(66)}$ = 2.889, p = 0.0052), SP (Fig. 6G; extended data Fig. 6-2; t-test, $t_{(66)}$ = 4.595, p < 0.0001), and SR (Fig. 6G; extended data Fig. 6-2; t-test, $t_{(66)}$ = 4.727, p < 0.0001) layers of CA1 hippocampus. Interestingly, vGlut1-positive excitatory presynaptic

boutons onto PV inhibitory neurons were also reduced in KO mice, specifically in the SO (Fig. 6I; extended data Fig. 6-2; t-test, t-test; $t_{(48)} = 5.536$, $p < 0.0001$) and SP (Fig. 6I; extended data Fig. 6-2; t-test, $t_{(67)} = 6.349$, $p < 0.0001$), but not in the SR (Fig. 6I; extended data Fig. 6-2; t-test, $t_{(20)} = 0.2142$, $p = 0.8325$) layers of CA1 hippocampus. The reduced excitatory drive onto PV inhibitory neurons in the CA1 hippocampus may contribute to the reduced number of PV expressing cells, lower number of inhibitory synapses in the SP and SO layers of the CA1 hippocampus and lower inhibitory activity, resulting in an overall increase in E/I balance in astrocyte-specific ephrin-B1 KO mice.

**Astrocytic ephrin-B1 KO mice show impaired social behaviors, but no anxiety or hyperactivity.**

Altered E/I balance as a result of aberrant excitatory and inhibitory synapse development is also observed in several ASD mouse models (Lee et al., 2017) and may underlie changes in ASD-like behaviors, such as social novelty and preference, as well as anxiety and hyperactivity. As deletion of astrocytic ephrin-B1 occurs globally in KO mice generated in these study, it is possible that the changes in E/I balance that we see in the hippocampus may not be exclusive to this area of the brain. Considering that ephrins and Eph receptors are identified as risk genes for the development of ASD in humans (Sanders et al., 2012), we also analyzed ASD-like behaviors. Moreover, social memory has been linked to hippocampus function as well (Hitti and Siegelbaum, 2014; Ko, 2017). Social novelty and social preference were assessed using a three-chamber test using group 1 KO male mice and their controls. Mice were placed in a cage containing two side chambers and were tested in two 10-min sessions. In session one, an unfamiliar stranger mouse (S1) was placed in one of the side chambers, with the other chamber

remaining empty (Fig. 7A). Control mice spent significantly more time in the chamber with S1 than the empty chamber (two-way ANOVA, Tukey's post hoc test, $p < 0.0001$) or the middle chamber (two-way ANOVA, Tukey's post hoc test, $p = 0.0002$); however, KO mice spent similar amount of time in each chamber, indicating impaired social preference (Fig. 7B; extended data Fig. 7-1). In session two, a novel mouse (S2) was placed in the empty chamber, while now familiar S1 mouse was remained in the same chamber. This test assessed social preferences by measuring the time that the mouse spent with either the familiar S1 mouse or a novel S2 mouse (Fig. 7A). Control mice spent significantly more time in the chamber with the novel S2 mouse than the familiar S1 mouse (two-way ANOVA, Tukey's post hoc test, $p = 0.0005$) or the middle chamber (two-way ANOVA, Tukey's post hoc test, $p = 0.0080$, Fig. 7C; extended data Fig. 7-2). However, KO mice spent the same amount of time in the chamber containing S1 mouse, S2 mouse, or the middle chamber, suggesting they could not discriminate between a familiar and novel mouse. Further, the social preference and social novelty index was calculated to directly measure the differences between control and KO mice; KO mice had a significantly lower social preference index (Fig. 7D; extended data Fig. 7-3; t-test, $t_{(14)} = 3.337$, $p = 0.0049$). A value near 1 indicates more time spent with the S1 chamber while a value near 0.5 indicates equal amount of time spent in both S1 and empty chamber. The social preference index of KO was near 0.5, indicating impaired social preference, spending equal amount of time between an empty chamber and a chamber with a stranger mouse. The social novelty index was also significantly lower in KO mice (Fig. 7E; extended data Fig. 7-3; t-test, $t_{(14)} = 2.661$, $p = 0.0186$). Social novelty index of WT mice is near 1 indicating more time spent in S2 chamber with a novel mouse than in S1 chamber with the familiar mouse. The social novelty index of KO mice is near 0.5 indicating a deficit in social memory.

Anxiety and hyperexcitability were assessed group 1 KO mice and their controls using an open field test (Fig. 7F) by determining the time mice spent in thigmotaxis (near the walls) and the average velocity of the mice. Both control and KO mice exhibited similar time spent in thigmotaxis (Fig. 7G; extended data Fig. 7-4; t-test, $t_{(15)} = 0.3455$, $p = 0.7345$), indicating no changes in anxious behavior following ephrin-B1 KO in astrocytes. Average velocity across the entire test was also similar between control and KO mice (Fig. 7H; extended data Fig. 7-4; t-test, $t_{(15)} = 0.1.214$, $p = 0.2435$), suggesting no signs of hyperactivity.

**Discussion**

Interactions between neurons and astrocytes are essential for proper circuit formation, particularly during early postnatal development when synapses are rapidly forming and being eliminated. The studies presented here suggest that astrocytic ephrin-B1 regulates hippocampal excitatory/inhibitory balance by negatively influencing excitatory synapse formation and enhancing inhibition during early postnatal development. First, we found that loss of ephrin-B1 in astrocytes enhances excitability of CA1 hippocampal neurons. We observed increased evoked AMPAR- and NMDAR-mediated responses, increased excitatory synapse numbers and higher dendritic spines density in CA1 neurons following the deletion of ephrin-B1 from astrocytes during P14-P28 period. In contrast, overexpression of astrocytic ephrin-B1 during the same period resulted in reduced evoked AMPAR- and NMDAR-mediated EPSCs. Second, evoked inhibitory responses were decreased in CA1 neurons of KO mice, most likely due to lower density of PV-expressing inhibitory neurons and a reduction of inhibitory synapses on CA1 pyramidal neurons in the SP and SO areas. In contrast, evoked IPSCs were enhanced on excitatory CA1 pyramidal cells following ephrin-B1 overexpression in developing astrocytes.

Third, loss of astrocytic ephrin-B1 during postnatal development impaired mouse social behaviors**.** Together, these studies implicate astrocytic ephrin-B1 in developmental refinement of neuronal circuits.

Eph/ephrin signaling has been shown to modulate synapse development both *in vitro* and *in vivo* (Ethell et al., 2001; Henderson et al., 2001; Takasu et al., 2002; Henkemeyer et al., 2003; Liebl et al., 2003). Eph/ephrin-B signaling is involved in both presynaptic and postsynaptic differentiation and function. Presynaptic ephrin-Bs, specifically ephrin-B1 and B2, interact with postsynaptic EphB2 to induce formation of functional presynaptic release sites on axons (Kayser et al., 2006; McClelland et al., 2009). Postsynaptically, Eph/ephrin-B signaling can affect synaptic plasticity, spinogenesis, glutamate receptor recruitment, and synapse density (Dalva et al., 2000; Ethell et al., 2001; Grunwald et al., 2001; Contractor et al., 2002; Henkemeyer et al., 2003; Grunwald et al., 2004; McClelland et al., 2010; Xu et al., 2011). Eph/ephrin-B signaling is also implicated in synaptic function (Essmann et al., 2008) Essmann et al., 2008). However, the mechanism of astrocyte-neuron Eph/ephrin-B signaling may differ from neuron-neuron signaling. In contrast to neuronal Eph/ephrin-B signaling, we observed enhanced excitatory synapse number and function with the loss of astrocytic ephrin-B1 and conversely, reduced excitatory synapse numbers following the overexpression of ephrin-B1. It is possible that astrocytic ephrin-B1 can inhibit synapse formation by interfering with the interactions between axon terminals of CA3 neurons and postsynaptic dendrites of CA1 neurons. Indeed, we observed a re-distribution of neuronal ephrin-B1 from cell body of CA1 neurons to dendrites following the deletion of ephrin-B1 from astrocytes, potentially increasing its interactions with EphB receptors at CA3 neuron terminals. Astrocytic ephrin-B1 can also induce removal of excess synapses via phagocytic mechanisms (Gong et al., 2019). As astrocytes are involved in

synapse elimination via phagocytosis (Chung et al., 2013), astrocytic elimination of excess synapses may be mediated by Eph/ephrin signaling during early postnatal development. Interestingly, despite increased excitatory synapse number, loss of ephrin-B1 in developing astrocytes does not affect AMPAR/NMDAR EPSC ratio and the levels of synaptic AMPARs, suggesting no changes in functional synapse maturation. However, loss of ephrin-B1 in astrocytes during development may result in delayed structural maturation as KO neurons have significantly more spines with smaller heads.

In addition, decreased inhibitory transmission in CA1 pyramidal neurons may also contribute to their enhanced excitability in astrocyte-specific ephrin-B1 KO mice. Astrocytes co-cultured with developing neurons have been shown to significantly increase GABAergic synaptogenesis (Hughes et al., 2010) and increase amplitude and density of $GABA_A$ currents (Liu et al., 1996; Elmariah et al., 2005). Interestingly, neuronal cell bodies that were in direct contact with astrocytes exhibited higher amplitude and density of $GABA_A$ current (Liu et al., 1996). The increase in number of inhibitory presynaptic terminals, frequency of mIPSCs, and synaptic localization of $GABA_A$ receptor clusters was observed in neuronal co-cultures with astrocytes (Elmariah et al., 2005), but was not mediated by astrocyte-derived thrombospondins (Hughes et al., 2010). Our studies show that the loss of astrocytic ephrin-B1 in the developing hippocampus leads to decreased inhibitory responses in CA1 hippocampal neurons potentially due to decreased number of PV-expressing inhibitory neurons (Fig. 8). Additionally, we observed a reduced number of excitatory vGlut1-positive puncta on PV cells in CA1 hippocampus of KO mice, suggesting decreased excitatory drive onto PV-expressing neurons, which may lead to a reduced expression of PV, therefore affecting their functions. Ephrin-B has been implicated in the neurogenesis of inhibitory neurons in the hippocampus (Talebian et al.,

2018). Deletion of ephrin-B during embryogenesis affects the migration of interneurons thereby reducing the number of interneurons and increasing the excitation of cortical networks (Talebian et al., 2017). Inhibitory neurons, in particular PV-expressing interneurons, are generated during embryonic development (Butt et al., 2005; Miyoshi et al., 2010; Tricoire et al., 2011) and migrate into the hippocampus by E14 (Tricoire et al., 2011). However, the expression of PV in interneurons is minimal until P12 and is gradually increases until P30 (Nitsch et al., 1990; de Lecea et al., 1995), which coincides with the maturation of inhibitory neurons in rat hippocampus (Michelson and Lothman, 1989). In our study, ephrin-B1 was deleted from astrocytes during P14-P28 period of PV cell maturation. As expression of PV is still increasing during this period in an activity dependent manner, the loss astrocytic ephrin-B1 may be affecting the maturation of inhibitory circuits in the CA1 hippocampus by influencing excitatory innervation of PV inhibitory neurons (Fig. 8).

Although astrocytic ephrin-B1 may play a similar role as a negative regulator of excitatory synapse formation during development and adulthood (Koeppen et al., 2018), its role in inhibitory neurons is different in developing and adult hippocampus. In contrast to early postnatal development, deletion of astrocytic ephrin-B1 in the adult hippocampus does not affect IPSCs (Nguyen et al., 2020). In the adult hippocampus, inhibitory neurons are mature and have distinct properties (Wamsley and Fishell, 2017); therefore, fully established inhibitory neurons may require different astrocytic signaling for proper function. The exact role of Eph/ephrin signaling in interneurons is still unknown; further investigation is required to determine how Eph/ephrin signaling mediates interneuron maturation and function, and specifically how astrocytes may contribute to these mechanisms. Interestingly, ephrin-B signaling in astrocytes is shown to regulate neurogenesis in the dentate gyrus (DG) of the hippocampus (Ashton et al.,

2012). EphB1 is also found to regulate cell number, proliferation, and positioning of neural stem and progenitor cells in the DG (Chumley et al., 2007). However, ephrin-B1 overexpression only in CA1 hippocampal astrocytes during P14-P28 period resulted in increased evoked IPSCs recorded from CA1 neurons, suggesting that the changes that we observe in our study are independent of neuronal differentiation in DG. Therefore, astrocytic ephrin-B1 may be essential in maintaining proper E/I balance by influencing PV cell development in the developing hippocampus. Furthermore, we observed the effects of astrocytic ephrin-B1 deletion on inhibitory function during P14-P28 period, but not in the adult hippocampus, suggesting the role of astrocytic ephrin-B1 in the maturation of inhibitory circuits in the developing hippocampus through yet unknown mechanisms.

We report that the loss of astrocytic ephrin-B1 enhanced excitatory function while also reducing inhibition. This E/I imbalance has been implicated in impaired sociability and social preference in the ASD mouse model (Lee et al., 2017). Aberrant synaptogenesis has been linked to several neurodevelopmental disorders, such as autism spectrum disorder and epilepsy (Huttenlocher and Dabholkar, 1997; Lillis et al., 2015; Shen et al., 2016). Additionally, PV interneurons have been shown to have tight control over excitatory cell firing rhythms as PV interneurons can generate highly synchronized and fast inhibitory patterns (Hu et al., 2014). Loss of PV interneurons may further contribute to the E/I imbalance and impaired social preference seen in astrocyte-specific ephrin-B1 KO mice. Indeed, loss of PV interneurons results in behavioral changes in mice similar core autism symptoms, including reduced social interactions and ultrasonic vocalizations, increased repetitive and stereotyped patterns of behaviors, impaired reversal learning and increased seizure susceptibility (Wohr et al., 2015). It is interesting to note these PV-depleted mice exhibited no impairments with motor function and no anxiety-like or

depression-like behaviors (Wohr et al., 2015). Blocking synaptic transmission of PV neurons specifically in the ventral hippocampus was also shown to impair social memory discrimination (Deng et al., 2019). Our findings show that loss of astrocytic ephrin-B1 reduced sociability but had no effect on anxiety or motor function. The observed reduction in density of PV-expressing neurons in astrocyte-specific ephrin-B1 KO mice is most likely not specific to the hippocampus as we also see the changes in social behaviors. Together, this suggests that targeting astrocytic ephrin-B1 may be a potential avenue to repair PV cell functions and restore E/I balance in neurodevelopmental disorders.

The studies presented here suggest that astrocytic ephrin-B1 regulates E/I balance in the CA1 hippocampus during early postnatal development. During P14-P28 developmental period, astrocytic ephrin-B1 negatively regulates excitatory synapse formation, as deletion of ephrin-B1 in astrocytes results in increased excitation (Fig. 8), while overexpression of ephrin-B1 in astrocytes decreases excitation of CA1 neurons potentially through enhanced synapse elimination. Astrocytic ephrin-B1 may also affect inhibitory neuron maturation and function as loss of astrocytic ephrin-B1 reduces density of PV-expressing inhibitory neurons in the CA1 hippocampus, and in turn impairs evoked IPSCs and mIPSC amplitude recorded from CA1 pyramidal neurons. Conversely, overexpression of ephrin-B1 in astrocytes enhances evoked IPSCs in CA1 neurons. The deregulation of E/I balance in astrocyte-specific ephrin-B1 KO mice may contribute to observed changes in social behaviors of the mice. Genetic studies have linked mutations associated with Eph/ephrin signaling with neurodevelopmental disorders, including autism spectrum disorders (Sanders et al., 2012; Robichaux et al., 2014), which are associated with social impairments and repetitive behaviors, as well as increased seizure susceptibility due to E/I imbalance (Gao and Penzes, 2015). Therefore, further understanding the role of astrocytic

862 ephrin-B1 in establishing proper E/I balance during development may provide a potential target
863 for treating neurodevelopmental disorders.
864

## References


Allen NJ, Eroglu C (2017) Cell Biology of Astrocyte-Synapse Interactions. Neuron 96:697-708.

Allen NJ, Bennett ML, Foo LC, Wang GX, Chakraborty C, Smith SJ, Barres BA (2012) Astrocyte glypicans 4 and 6 promote formation of excitatory synapses via GluA1 AMPA receptors. Nature 486:410-414.

Araque A, Parpura V, Sanzgiri RP, Haydon PG (1999) Tripartite synapses: glia, the unacknowledged partner. Trends Neurosci 22:208-215.

Ashton RS, Conway A, Pangarkar C, Bergen J, Lim KI, Shah P, Bissell M, Schaffer DV (2012) Astrocytes regulate adult hippocampal neurogenesis through ephrin-B signaling. Nat Neurosci 15:1399-1406.

Beattie EC, Stellwagen D, Morishita W, Bresnahan JC, Ha BK, Von Zastrow M, Beattie MS, Malenka RC (2002) Control of synaptic strength by glial TNFalpha. Science 295:2282-2285.

Bonansco C, Fuenzalida M (2016) Plasticity of Hippocampal Excitatory-Inhibitory Balance: Missing the Synaptic Control in the Epileptic Brain. Neural Plast 2016:8607038.

Bush JO, Soriano P (2009) Ephrin-B1 regulates axon guidance by reverse signaling through a PDZ-dependent mechanism. Genes Dev 23:1586-1599.

Butt SJ, Fuccillo M, Nery S, Noctor S, Kriegstein A, Corbin JG, Fishell G (2005) The temporal and spatial origins of cortical interneurons predict their physiological subtype. Neuron 48:591-604.

Castaneda-Castellanos DR, Flint AC, Kriegstein AR (2006) Blind patch clamp recordings in embryonic and adult mammalian brain slices. Nat Protoc 1:532-542.

886 Christopherson KS, Ullian EM, Stokes CC, Mullowney CE, Hell JW, Agah A, Lawler J, Mosher
887 DF, Bornstein P, Barres BA (2005) Thrombospondins are astrocyte-secreted proteins that
888 promote CNS synaptogenesis. Cell 120:421-433.
889 Chumley MJ, Catchpole T, Silvany RE, Kernie SG, Henkemeyer M (2007) EphB receptors
890 regulate stem/progenitor cell proliferation, migration, and polarity during hippocampal
891 neurogenesis. J Neurosci 27:13481-13490.
892 Chung WS, Clarke LE, Wang GX, Stafford BK, Sher A, Chakraborty C, Joung J, Foo LC,
893 Thompson A, Chen C, Smith SJ, Barres BA (2013) Astrocytes mediate synapse elimination
894 through MEGF10 and MERTK pathways. Nature 504:394-400.
895 Clarke LE, Barres BA (2013) Emerging roles of astrocytes in neural circuit development. Nat
896 Rev Neurosci 14:311-321.
897 Contractor A, Rogers C, Maron C, Henkemeyer M, Swanson GT, Heinemann SF (2002) Trans-
898 synaptic Eph receptor-ephrin signaling in hippocampal mossy fiber LTP. Science 296:1864-
899 1869.
900 Dalva MB, Takasu MA, Lin MZ, Shamah SM, Hu L, Gale NW, Greenberg ME (2000) EphB
901 receptors interact with NMDA receptors and regulate excitatory synapse formation. Cell
902 103:945-956.
903 de Lecea L, del Rio JA, Soriano E (1995) Developmental expression of parvalbumin mRNA in
904 the cerebral cortex and hippocampus of the rat. Brain Res Mol Brain Res 32:1-13.
905 Deng X, Gu L, Sui N, Guo J, Liang J (2019) Parvalbumin interneuron in the ventral
906 hippocampus functions as a discriminator in social memory. Proc Natl Acad Sci U S A
907 116:16583-16592.

908 Elmariah SB, Oh EJ, Hughes EG, Balice-Gordon RJ (2005) Astrocytes regulate inhibitory
909 synapse formation via Trk-mediated modulation of postsynaptic GABAA receptors. J Neurosci
910 25:3638-3650.
911 Essmann CL, Martinez E, Geiger JC, Zimmer M, Traut MH, Stein V, Klein R, Acker-Palmer A
912 (2008) Serine phosphorylation of ephrinB2 regulates trafficking of synaptic AMPA receptors.
913 Nat Neurosci 11:1035-1043.
914 Ethell IM, Irie F, Kalo MS, Couchman JR, Pasquale EB, Yamaguchi Y (2001) EphB/syndecan-2
915 signaling in dendritic spine morphogenesis. Neuron 31:1001-1013.
916 Fellin T, Pascual O, Gobbo S, Pozzan T, Haydon PG, Carmignoto G (2004) Neuronal synchrony
917 mediated by astrocytic glutamate through activation of extrasynaptic NMDA receptors. Neuron
918 43:729-743.
919 Fritschy JM (2008) Epilepsy, E/I Balance and GABA(A) Receptor Plasticity. Frontiers in
920 molecular neuroscience 1:5.
921 Gao R, Penzes P (2015) Common mechanisms of excitatory and inhibitory imbalance in
922 schizophrenia and autism spectrum disorders. Curr Mol Med 15:146-167.
923 Gong J, Gaitanos TN, Luu O, Huang Y, Gaitanos L, Lindner J, Winklbauer R, Klein R (2019)
924 Gulp1 controls Eph/ephrin trogocytosis and is important for cell rearrangements during
925 development. J Cell Biol 218:3455-3471.
926 Grunwald IC, Korte M, Wolfer D, Wilkinson GA, Unsicker K, Lipp HP, Bonhoeffer T, Klein R
927 (2001) Kinase-independent requirement of EphB2 receptors in hippocampal synaptic plasticity.
928 Neuron 32:1027-1040.

929 Grunwald IC, Korte M, Adelmann G, Plueck A, Kullander K, Adams RH, Frotscher M,
930 Bonhoeffer T, Klein R (2004) Hippocampal plasticity requires postsynaptic ephrinBs. Nat
931 Neurosci 7:33-40.
932 Hama H, Hara C, Yamaguchi K, Miyawaki A (2004) PKC signaling mediates global
933 enhancement of excitatory synaptogenesis in neurons triggered by local contact with astrocytes.
934 Neuron 41:405-415.
935 Henderson JT, Georgiou J, Jia Z, Robertson J, Elowe S, Roder JC, Pawson T (2001) The
936 receptor tyrosine kinase EphB2 regulates NMDA-dependent synaptic function. Neuron 32:1041-
937 1056.
938 Henkemeyer M, Itkis OS, Ngo M, Hickmott PW, Ethell IM (2003) Multiple EphB receptor
939 tyrosine kinases shape dendritic spines in the hippocampus. J Cell Biol 163:1313-1326.
940 Henneberger C, Papouin T, Oliet SH, Rusakov DA (2010) Long-term potentiation depends on
941 release of D-serine from astrocytes. Nature 463:232-236.
942 Hitti FL, Siegelbaum SA (2014) The hippocampal CA2 region is essential for social memory.
943 Nature 508:88-92.
944 Hollingsworth EB, McNeal ET, Burton JL, Williams RJ, Daly JW, Creveling CR (1985)
945 Biochemical characterization of a filtered synaptoneurosome preparation from guinea pig
946 cerebral cortex: cyclic adenosine 3':5'-monophosphate-generating systems, receptors, and
947 enzymes. J Neurosci 5:2240-2253.
948 Hu H, Gan J, Jonas P (2014) Interneurons. Fast-spiking, parvalbumin(+) GABAergic
949 interneurons: from cellular design to microcircuit function. Science 345:1255263.

Hughes EG, Elmariah SB, Balice-Gordon RJ (2010) Astrocyte secreted proteins selectively increase hippocampal GABAergic axon length, branching, and synaptogenesis. Mol Cell Neurosci 43:136-145.

Hussain NK, Thomas GM, Luo J, Huganir RL (2015) Regulation of AMPA receptor subunit GluA1 surface expression by PAK3 phosphorylation. Proc Natl Acad Sci U S A 112:E5883-5890.

Huttenlocher PR, Dabholkar AS (1997) Regional differences in synaptogenesis in human cerebral cortex. J Comp Neurol 387:167-178.

Kaidanovich-Beilin O, Lipina T, Vukobradovic I, Roder J, Woodgett JR (2011) Assessment of social interaction behaviors. Journal of visualized experiments : JoVE.

Kayser MS, McClelland AC, Hughes EG, Dalva MB (2006) Intracellular and trans-synaptic regulation of glutamatergic synaptogenesis by EphB receptors. J Neurosci 26:12152-12164.

Ko J (2017) Neuroanatomical Substrates of Rodent Social Behavior: The Medial Prefrontal Cortex and Its Projection Patterns. Frontiers in neural circuits 11:41.

Koeppen J, Nguyen AQ, Nikolakopoulou AM, Garcia M, Hanna S, Woodruff S, Figueroa Z, Obenaus A, Ethell IM (2018) Functional Consequences of Synapse Remodeling Following Astrocyte-Specific Regulation of Ephrin-B1 in the Adult Hippocampus. J Neurosci 38:5710-5726.

Kucukdereli H, Allen NJ, Lee AT, Feng A, Ozlu MI, Conatser LM, Chakraborty C, Workman G, Weaver M, Sage EH, Barres BA, Eroglu C (2011) Control of excitatory CNS synaptogenesis by astrocyte-secreted proteins Hevin and SPARC. Proc Natl Acad Sci U S A 108:E440-449.

Lee E, Lee J, Kim E (2017) Excitation/Inhibition Imbalance in Animal Models of Autism Spectrum Disorders. Biological psychiatry 81:838-847.

973 Liebl DJ, Morris CJ, Henkemeyer M, Parada LF (2003) mRNA expression of ephrins and Eph
974 receptor tyrosine kinases in the neonatal and adult mouse central nervous system. Journal of
975 neuroscience research 71:7-22.
976 Lillis KP, Wang Z, Mail M, Zhao GQ, Berdichevsky Y, Bacskai B, Staley KJ (2015) Evolution
977 of Network Synchronization during Early Epileptogenesis Parallels Synaptic Circuit Alterations.
978 J Neurosci 35:9920-9934.
979 Liu QY, Schaffner AE, Li YX, Dunlap V, Barker JL (1996) Upregulation of GABAA current by
980 astrocytes in cultured embryonic rat hippocampal neurons. J Neurosci 16:2912-2923.
981 Lovelace JW, Rais M, Palacios AR, Shuai XS, Bishay S, Popa O, Pirbhoy PS, Binder DK,
982 Nelson DL, Ethell IM, Razak KA (2020) Deletion of Fmr1 from Forebrain Excitatory Neurons
983 Triggers Abnormal Cellular, EEG, and Behavioral Phenotypes in the Auditory Cortex of a
984 Mouse Model of Fragile X Syndrome. Cereb Cortex 30:969-988.
985 Mayford M, Siegelbaum SA, Kandel ER (2012) Synapses and memory storage. Cold Spring
986 Harb Perspect Biol 4.
987 McClelland AC, Sheffler-Collins SI, Kayser MS, Dalva MB (2009) Ephrin-B1 and ephrin-B2
988 mediate EphB-dependent presynaptic development via syntenin-1. Proc Natl Acad Sci U S A
989 106:20487-20492.
990 McClelland AC, Hruska M, Coenen AJ, Henkemeyer M, Dalva MB (2010) Trans-synaptic
991 EphB2-ephrin-B3 interaction regulates excitatory synapse density by inhibition of postsynaptic
992 MAPK signaling. Proc Natl Acad Sci U S A 107:8830-8835.
993 Michelson HB, Lothman EW (1989) An in vivo electrophysiological study of the ontogeny of
994 excitatory and inhibitory processes in the rat hippocampus. Brain research Developmental brain
995 research 47:113-122.

996 Miyoshi G, Hjerling-Leffler J, Karayannis T, Sousa VH, Butt SJ, Battiste J, Johnson JE,
997 Machold RP, Fishell G (2010) Genetic fate mapping reveals that the caudal ganglionic eminence
998 produces a large and diverse population of superficial cortical interneurons. J Neurosci 30:1582-
999 1594.
1000 Moeller ML, Shi Y, Reichardt LF, Ethell IM (2006) EphB receptors regulate dendritic spine
1001 morphogenesis through the recruitment/phosphorylation of focal adhesion kinase and RhoA
1002 activation. J Biol Chem 281:1587-1598.
1003 Nguyen AQ, Koeppen J, Woodruff S, Mina K, Figueroa Z, Ethell IM (2020) Astrocytic Ephrin-
1004 B1 Controls Synapse Formation in the Hippocampus During Learning and Memory. Front
1005 Synaptic Neurosci 12:10.
1006 Nitsch R, Soriano E, Frotscher M (1990) The parvalbumin-containing nonpyramidal neurons in
1007 the rat hippocampus. Anatomy and embryology 181:413-425.
1008 Nolt MJ, Lin Y, Hruska M, Murphy J, Sheffler-Colins SI, Kayser MS, Passer J, Bennett MV,
1009 Zukin RS, Dalva MB (2011) EphB controls NMDA receptor function and synaptic targeting in a
1010 subunit-specific manner. J Neurosci 31:5353-5364.
1011 Nygaard KR, Maloney SE, Dougherty JD (2019) Erroneous inference based on a lack of
1012 preference within one group: Autism, mice, and the social approach task. Autism research :
1013 official journal of the International Society for Autism Research 12:1171-1183.
1014 Robichaux MA, Chenaux G, Ho HY, Soskis MJ, Dravis C, Kwan KY, Šestan N, Greenberg ME,
1015 Henkemeyer M, Cowan CW (2014) EphB receptor forward signaling regulates area-specific
1016 reciprocal thalamic and cortical axon pathfinding. Proc Natl Acad Sci U S A 111:2188-2193.
1017 Sanders SJ et al. (2012) De novo mutations revealed by whole-exome sequencing are strongly
1018 associated with autism. Nature 485:237-241.

1019 Segura I, Essmann CL, Weinges S, Acker-Palmer A (2007) Grb4 and GIT1 transduce ephrinB
1020 reverse signals modulating spine morphogenesis and synapse formation. Nat Neurosci 10:301-
1021 310.
1022 Shen Y, Qin H, Chen J, Mou L, He Y, Yan Y, Zhou H, Lv Y, Chen Z, Wang J, Zhou YD (2016)
1023 Postnatal activation of TLR4 in astrocytes promotes excitatory synaptogenesis in hippocampal
1024 neurons. J Cell Biol 215:719-734.
1025 Sloniowski S, Ethell IM (2012) Looking forward to EphB signaling in synapses. Semin Cell Dev
1026 Biol 23:75-82.
1027 Stellwagen D, Malenka RC (2006) Synaptic scaling mediated by glial TNF-alpha. Nature
1028 440:1054-1059.
1029 Südhof TC, Malenka RC (2008) Understanding synapses: past, present, and future. Neuron
1030 60:469-476.
1031 Takasu MA, Dalva MB, Zigmond RE, Greenberg ME (2002) Modulation of NMDA receptor-
1032 dependent calcium influx and gene expression through EphB receptors. Science 295:491-495.
1033 Talebian A, Britton R, Henkemeyer M (2018) Abnormalities in cortical interneuron subtypes in
1034 ephrin-B mutant mice. Eur J Neurosci 48:1803-1817.
1035 Talebian A, Britton R, Ammanuel S, Bepari A, Sprouse F, Birnbaum SG, Szabo G, Tamamaki
1036 N, Gibson J, Henkemeyer M (2017) Autonomous and non-autonomous roles for ephrin-B in
1037 interneuron migration. Dev Biol 431:179-193.
1038 Tricoire L, Pelkey KA, Erkkila BE, Jeffries BW, Yuan X, McBain CJ (2011) A blueprint for the
1039 spatiotemporal origins of mouse hippocampal interneuron diversity. J Neurosci 31:10948-10970.
1040 Ullian EM, Sapperstein SK, Christopherson KS, Barres BA (2001) Control of synapse number
1041 by glia. Science 291:657-661.

1042 Wamsley B, Fishell G (2017) Genetic and activity-dependent mechanisms underlying
1043 interneuron diversity. Nat Rev Neurosci 18:299-309.
1044 Wohr M, Orduz D, Gregory P, Moreno H, Khan U, Vorckel KJ, Wolfer DP, Welzl H, Gall D,
1045 Schiffmann SN, Schwaller B (2015) Lack of parvalbumin in mice leads to behavioral deficits
1046 relevant to all human autism core symptoms and related neural morphofunctional abnormalities.
1047 Translational psychiatry 5:e525.
1048 Xu NJ, Henkemeyer M (2012) Ephrin reverse signaling in axon guidance and synaptogenesis.
1049 Semin Cell Dev Biol 23:58-64.
1050 Xu NJ, Sun S, Gibson JR, Henkemeyer M (2011) A dual shaping mechanism for postsynaptic
1051 ephrin-B3 as a receptor that sculpts dendrites and synapses. Nat Neurosci 14:1421-1429.
1052 Yan QJ, Rammal M, Tranfaglia M, Bauchwitz RP (2005) Suppression of two major Fragile X
1053 Syndrome mouse model phenotypes by the mGluR5 antagonist MPEP. Neuropharmacology
1054 49:1053-1066.
1055 Yan QJ, Asafo-Adjei PK, Arnold HM, Brown RE, Bauchwitz RP (2004) A phenotypic and
1056 molecular characterization of the fmr1-tm1Cgr fragile X mouse. Genes Brain Behav 3:337-359.
1057 Zimmer M, Palmer A, Kohler J, Klein R (2003) EphB-ephrinB bi-directional endocytosis
1058 terminates adhesion allowing contact mediated repulsion. Nat Cell Biol 5:869-878.
1059

1060 **Figure Legends**

1061 **Figure 1 Postnatal deletion of astrocytic ephrin-B1 results in enhanced excitation of CA1**
1062 **hippocampal neurons.** (A) Timeline of tamoxifen injection; 50 mg of tamoxifen was
1063 intraperitoneally injected at P14 for five days, experiments were performed at P28, fourteen days
1064 after initial injection. Three transgenic mice groups were used in this study: (1) ERT2-Cre$^{GFAP}$

(Control) and ERT2-Cre$^{GFAP}$ephrin-B1$^{flox/y}$ (KO); (2) tdTomato- ERT2-Cre$^{GFAP}$ (Control) and tdTomato-ERT2-Cre$^{GFAP}$ephrin-B1$^{flox/y}$ (KO) and (3) Thy1-GFP- ERT2-Cre$^{GFAP}$ (Control) and tdTomato-ERT2-Cre$^{GFAP}$ephrin-B1$^{flox/y}$ (KO). (B) Schematic representation of mouse hippocampus with cornu ammonis (CA), dentate gyrus (DG) and hippocampal layers: stratum oriens (SO), stratum pyramidale (SP), stratum radiatum (SR), and stratum lacunosum moleculare (SLM). Outlined box indicates areas analyzed in these studies. (C, D) Max projection confocal images show astrocytes expressing tdTomato (red) and ephrin-B1 immunoreactivity (green) with DAPI (blue) in the CA1 hippocampus of group 2 control and KO mice, scale bar is 200 µm. High magnification images show examples of ephrin-B1 immunoreactivity in astrocytes (asterisk), and cell body (arrowhead) or dendrites (arrow) of CA1 neurons, scale bar is 20 µm. (E) Ephrin-B1 immunoreactivity was significantly reduced in the astrocytes of CA1 hippocampus in KO mice as compared to control mice (left panel, n = 8-10, t-test, * $p<0.05$; Fig. 1-1). Ephrin-B1 immunoreactivity was also significantly reduced in the cell body of CA1 neurons (middle panel, n=8-12, t-test, $p<0.0001$; Fig. 1-1), but was upregulated in proximal dendrites of CA1 neurons (right panel, t-test, n=15-18, $p<0.0001$; Fig. 1-1). (F-H) Input-output curves of CA1 neuronal FV amplitude (F), fEPSP slope (G), and PS amplitude (H) as a function of increasing stimulation intensity of Schaffer collaterals in hippocampal slices from group 1 control and KO mice. Deletion of astrocytic ephrin-B1 resulted in increased fEPSP slope and PS amplitude following stimulation of Schaffer collaterals (n = 6-9 mice; two-way ANOVA followed by Bonferroni post-test; Fig. 1-2, 1-3). Graphs show mean and error bars represent SEM; * $p<0.05$, ** $p<0.01$.

**Figure 2 Loss of astrocytic ephrin-B1 during early postnatal development enhances both AMPAR and NMDAR-mediated responses but not AMPAR/NMDAR EPSC ratio.** (A) Whole cell recordings were performed by blind cell patching of pyramidal cells in the CA1 hippocampus (example of biocytin filled neuron). (B) Representative traces of AMPAR- and NMDAR-evoked responses in control (gray) and KO (black) mice in the presence of picrotoxin to block GABAergic inhibition. (C, D) Graphs show amplitude and corresponding ratio of AMPAR- and NMDAR-mediated currents (n = 10-11 cells, 6-7 mice; Fig. 2-1). Evoked AMPAR- and NMDAR-mediated currents were significantly increased; however, ratio was unchanged. (E) Representative traces of mEPSCs in P28 control and KO mice; recorded in the presence of TTX and picrotoxin (n = 5 mice). (F) The cumulative distribution of mEPSC inter-event intervals shows no differences between control and KO mice. (G) Average frequency of mEPSCs was not significantly different between control and KO mice, indicating potentially no effect on pre-synaptic activity (Fig. 2-1). (H) The cumulative distribution of mEPSC amplitude shows a significant rightward shift (higher mESPC amplitude across the distribution) for KO (black) mice compared to control (gray). (I) Average amplitude of mEPSCs was higher in KO compared to control mice (Fig. 2-1). Graphs show mean and error bars represent SEM; t-test, * $p<0.05$, ** $p<0.01$.

**Figure 3 Overexpression of astrocytic ephrin-B1 in the developing hippocampus reduced evoked AMPAR- and NMDAR-mediated responses.**

(A) Timeline of the VP injection: AAV-ephrin-B1 or AAV-tdTomato was stereotaxically injected unilaterally in the dorsal hippocampus at P14; experiments were performed at P28, fourteen days after injection. (B-C) Max projection confocal images show GFAP (red) and

ephrin-B1 (green) immunoreactivity with DAPI (blue) in the ipsilateral CA1 hippocampus injected with AAV-ephrin-B1 (OE) and contralateral non-injected CA1 hippocampus (Control), scale bar is 200 µm. High magnification images show examples of ephrin-B1 immunoreactivity in astrocytes and neuronal cell bodies in SO, SP and SR layers of CA1 hippocampus, scale bar is 20 µm. (D) Ephrin-B1 immunoreactivity was significantly increased in all layers of CA1 hippocampus in ipsilateral CA1 hippocampus injected with AAV-ephrin-B1 (OE) compared to contralateral non-injected CA1 hippocampus (Control) (n = 11-13, t-test, *** $p<0.001$; ****$p<0.0001$; Fig. 3-1). (E) For electrophysiology, control group included recordings from ipsilateral side of AAV-tdTomato injected mice and contralateral side of AAV-ephrin-B1 injected mice. Overexpressing group (OE) included recordings from ipsilateral side of AAV-ephrin-B1 injected mice. Representative traces of AMPAR- and NMDAR-evoked responses in CA1 hippocampal neurons of control (gray) and OE (dotted dark gray) P28 hippocampus with whole-cell recording in the presence of picrotoxin to block GABAergic inhibition. (F, G) Graphs show amplitude and corresponding ratio in AMPAR- and NMDAR-mediated currents (n = 11-14 cells, 5 mice per group; Fig. 3-2). Evoked AMPAR and NMDAR-mediated currents were significantly decreased; however, ratio was unchanged. (H) Representative traces of mEPSCs in CA1 hippocampal neurons of P28 control and OE hippocampus; whole-cell recording was done in the presence of TTX and picrotoxin (n = 11-14 cells, 5 mice per group). (I) The cumulative distribution of mEPSC inter-event intervals in control (black) and OE (gray) groups. (J) Average frequency of mEPSCs was not significantly different between control and OE groups, indicating potentially no effect on pre-synaptic activity (Fig. 3-2). (K) The cumulative distribution of mEPSC amplitude shows a significant leftward shift (smaller mESPC amplitude across the distribution) for OE (dotted dark gray) compared to control group (gray). (L) Average amplitude

of mEPSCs was lower in OE compared to control group (Fig. 3-2). Graphs show mean and error bars represent SEM; t-test, * $p<0.05$, **$p<0.01$.

**Figure 4 Early postnatal astrocyte-specific deletion of ephrin-B1 resulted in increased number of excitatory synapses in CA1 hippocampus.** (A-B) Confocal images show vGlut1 (green) and PSD-95 (red) immunolabeling in SR and SLM areas of CA1 hippocampus of group 1 control and KO mice (scale bar = 25 μm). (C-E) Graphs show density of vGlut1-positive puncta (C), PSD95-positive puncta (D), and vGlut1/PSD95 co-localization (E) per 100 $\mu m^2$ of SR and SLM areas in CA1 hippocampus of control and KO mice (n = 3-4 mice; Fig. 4-1). KO mice showed a significant increase of vGlut1-positive puncta, PSD95-positive puncta, and the colocalization of vGlut1 and PSD95 in the SR CA1 hippocampus. Graphs show mean values and error bars represent SEM; ***$p<0.001$, ****$p<0.0001$. (F) Confocal images show dendrites of CA1 neurons expressing GFP in the SR area of CA1 hippocampus of control and KO mice (scale bar = 10 μm). (G-I) Graphs show average density of dendritic spines per 10 μm dendrite (G), average spine length (H), and spine volume (I). There was a significant increase in average dendritic spine density in KO mice compared to control mice (Fig. 4-2). There was a significantly increased proportion of dendritic spines with smaller heads (volume 0-0.5 $\mu m^3$), a decreased percent of medium size spines (volume 0.5-1.0 $\mu m^3$), and same percent of large, mature spines (volume >1.0 $\mu m^3$) observed in KO mice compared to control mice. Graphs show mean and error bars represent SEM; *$p < 0.05$, **$p < 0.01$, ****$p < 0.0001$ (Fig. 4-3). (K) Western blots show levels of PSD-95, GAPDH, and AMPAR subunits (GluA1 and GluA2/3) in synaptosomes isolated from hippocampus of P28 control and KO mice (Fig. 4-4). Graphs show mean ratios of synaptic PSD-95 to GAPDH, and GluA1, or GluA2/3 levels to PSD-95 levels in

synaptosomes isolated from P28 hippocampus of control and KO mice (Fig. 4-5). AMPAR levels at hippocampal synapses are similar in P28 control and KO mice. Graphs show mean and error bars represent SEM.

**Figure 5 Inhibition is altered in CA1 hippocampal neurons following deletion or overexpression of astrocytic ephrin-B1 during early postnatal development.** (A) Representative traces showing evoked IPSCs recorded in CA1 pyramidal neurons from group 1 control (gray) and KO (black); whole-cell recording was done in the presence of D-AP5 and NBQX to block AMPAR- and NMDAR-mediated currents. (B) Graph shows average amplitude of evoked IPSCs (n = 12-14 cells, 6 mice per group; Fig. 5-1). Amplitude of evoked IPSCs is significantly decreased in CA1 neurons of P28 KO mice compared to control mice. (C) Representative traces of mIPSCs in control and KO mice; whole-cell recording was done in the presence of NBQX, D-AP5, and TTX (n = 12-14 cells, 6 mice per group). (D) The cumulative distribution of mIPSC inter-event intervals in control (gray) and KO (black) mice. (E) Average frequency of mIPSCs was not significantly different between control and KO mice, indicating potentially no effect on pre-synaptic activity (Fig. 5-1). (F) The cumulative distribution of mIPSC amplitude shows a significant leftward shift (smaller mISPC amplitude across the distribution) for KO (black) mice compared to control (gray). (G) Average amplitude of mIPSCs was significantly lower in KO compared to control mice (Fig. 5-1). (H) Representative traces showing evoked IPSCs recorded in CA1 pyramidal neurons from P28 control (gray) and OE (dotted dark gray); whole-cell recording was done in the presence of D-AP5 and NBQX to block AMPAR- and NMDAR-mediated currents. (I) Graph shows average amplitude of evoked IPSCs (n = 10-11 cells, 6 mice per group; Fig. 5-2). Amplitude of evoked IPSCs was significantly

decreased in CA1 neurons of OE compared to control group. (J) Representative traces of mIPSCs in P28 control and OE groups; whole-cell recording was done in the presence of NBQX, D-AP5, and TTX (n = 10-11 cells, 6 mice per group). (K) The cumulative distribution of mIPSC inter-event intervals in control (gray) and OE (dotted dark gray) groups. There is a significant rightward shift in OE group, indicating larger inter-event intervals between spikes. (L) However, average frequency of mIPSCs was not significantly different between control and OE groups (Fig. 5-2). (M) The cumulative distribution of mIPSC amplitude in control (gray) compared to OE group (dotted dark gray). (N) Average amplitude of mIPSCs was similar between control and OE groups (Fig. 5-2). Graphs show mean and error bars represent SEM; t-test, *$p<0.05$.

**Figure 6 Inhibitory synaptic sites on the CA1 pyramidal neurons and the density of PV-expressing inhibitory neurons are reduced following the deletion of astrocytic ephrin-B1 during early postnatal development.** (A, B) Confocal images show CA1 excitatory neurons expressing GFP (green) co-stained with VGAT (red) and gephyrin (blue) to visualize inhibitory synaptic sites (scale bar = 50 μm). High magnification images show GFP-expressing dendrites (green) with VGAT (red) and gephyrin (purple; scale bar = 10 μm) (C-E) Graphs show VGAT/gephyrin co-localized puncta on GFP-expressing primary and secondary SR dendrites (C), neuronal cell bodies in SP (D) and SO dendrites (E) of CA1 neurons. KO mice exhibited a significant decrease in density of VGAT/gephyrin colocalized puncta on CA1 neurons in the SP and SO layers (n = 11-20 images; 4 mice per group, t-test $p<0.05$; Fig. 6-1). (F) Confocal images show PV-expressing cells (red) and DAPI staining (blue) to identify CA1 hippocampal layers, SO, SP, and SR. (G) Graph shows density of PV-expressing neurons in SO, SP, and SR layers of CA1 hippocampus. KO mice exhibited a significant decrease in density of PV-expressing

inhibitory neurons in all three layers (n = 30-35 images; 3 mice per group; t-test $p<0.01$, $p<0.0001$; Fig. 6-2). (H) Confocal images show vGlut1 immunoreactivity (green) on PV-expressing cells (red) in the SO, SP, and SR layers of the CA1 hippocampus (scale bar = 100 μm). (I) Graphs show co-localization of vGlut1 puncta and PV immunoreactivity in the SO, SP, and SR layers of the CA1 hippocampus (n = 10-40 cells, 3 mice per group; t-test $p<0.0001$; Fig. 6-2). KO mice exhibit decreased numbers of excitatory vGlut1-positive boutons on PV-expressing inhibitory neurons in the SO and SP of CA1 hippocampus. Graphs show mean and error bars represent SEM; *$p<0.05$, **$p<0.01$, ****$p<0.0001$.

**Figure 7 Ablation of astrocytic ephrin-B1 during early postnatal development affected mouse social behaviors.** (A) Diagram of three-chamber test for social preference and social novelty. Mice were placed in the middle chamber containing two side chambers and were tested in two 10 min sessions. During social preference test, a stranger mouse (S1) was placed in one of the side chambers, with the other chamber remaining empty. During social novelty test, now familiar stranger mouse (S1) remained in the side chamber, while a novel mouse (S2) was placed in the empty chamber. (B) Graph shows time spent in either three chambers during social preference test. Control mice prefer spending time with S1 mouse compared to time in the middle (two-way ANOVA, Tukey's post hoc test, $p = 0.0002$) or empty chamber (two-way ANOVA, Tukey's post hoc test, $p <0.0001$; Fig. 7-1). KO mice show impaired sociability and spend the same amount of time in each chamber. (C) Graph shows time spent in each chamber during social novelty test. Control mice spend significantly more time with novel S2 mouse than with familiar S1 mouse (two-way ANOVA, Tukey's post hoc test, $p = 0.0005$), or in the middle chamber (two-way ANOVA, Tukey's post hoc test, $p = 0.0080$; Fig. 7-2), indicating normal

social novelty. KO mice spend the same amount of time in S1, middle, or S2 chambers. (D) Graph shows social preference index, calculated as ($\frac{time\ in\ S1\ chamber}{time\ in\ S1\ chamber + time\ in\ empty\ chamber}$). KO mice show a significant reduction in social preference index (t-test, p = 0.0049), with a value near 0.5 indicating time spent between S1 chamber and the empty chamber was nearly equal (Fig. 7-3). (E) Graph shows social novelty index, calculated as ($\frac{time\ in\ S2\ chamber}{time\ in\ S2\ chamber + time\ in\ S1\ chamber}$). KO mice show a significant reduction in social novelty index (t-test, p = 0.0186), with a value near 0.5 indicating equal time spent between S2 and S1 chambers (Fig. 7-3). (F) Schematics of open field test; during testing animals were allowed to freely explore the open field for 10 min while time spent in thigmotaxis and average velocity were measured. (G) Graph shows percent time spent in thigmotaxis with no significant differences between control and KO mice (t-test, $t_{(15)}$ = 0.3455, p = 0.7345; Fig. 7-4). (H) Graph shows average velocity of control and KO mice (t-test, $t_{(15)}$ = 0.1.214, p = 0.2435; Fig. 7-4). Graphs show mean and error bars represent SEM; * p<0.05, **p<0.01, ***p<0.001, ****p<0.0001.

**Figure 8 Model schematic of hippocampal circuitry in control and KO mice.** (A) During P14- P28 period excitatory synapse formation on CA1 hippocampal neurons is reduced allowing for maturation and refinement of synaptic circuits through synapse elimination, while PV expression increases allowing for proper inhibition of excitatory cells. (B) Deletion of astrocytic ephrin-B1 affects E/I balance in the developing hippocampus, resulting in higher number of excitatory synapses onto CA1 pyramidal cells and reduced number of PV-expressing neurons in P28 hippocampus, thereby causing overall enhanced excitatory activity in the CA1 hippocampal pyramidal cells.

**Extended Data Legends**

Figure 1-1 Extended data and statistics for Figure 1E.

Figure 1-2 Extended data for Figure 1F-H.

Figure 1-3 Statistical data for Figure 1F-H.

Figure 2-1 Extended data and statistics for Figure 2C, D, G, I.

Figure 3-1 Extended data and statistics for Figure 3D.

Figure 3-2 Extended data and statistics for Figure 3E, F, G, J, L.

Figure 4-1 Extended data and statistics for Figure 4C-E.

Figure 4-2 Extended data and statistics for Figure 4G, H.

Figure 4-3 Extended data and statistics for Figure 4I.

Figure 4-4 Extended data for Figure 4K

(A) Western blot shows levels of PSD-95 and synapsin 1 in lysate and synaptosome fraction isolated from hippocampus of P28 mouse hippocampus. (B) Total levels of PSD-95 and synapsin 1 in lysates and synaptosome fractions isolated from P28 hippocampus of control and KO mice were analyzed confirming enrichment of synaptic proteins in a crude synaptosome fraction. Graphs show mean values and error bars represent SEM (n=4; PSD-95: t-test, $t_{(14)}$=4.598, p= 0.0004; Synapsin 1: Mann Whitney, unequal variance, Sum of ranks: 36, 100 Mann-Whitney U: 0, p= 0.0002).

Figure 4-5 Extended data and statistics for Figure 4K.

Figure 5-1 Extended data and statistics for Figure 5B, E, G.

Figure 5-2 Extended data and statistics for Figure 5I, L, N.

Figure 6-1 Extended data and statistics for Figure 6C, D, E.

Figure 6-2 Extended data and statistics for Figure 6G, I.

Figure 7-1 Extended data and statistics for Figure 7B.

Figure 7-2 Extended data and statistics for Figure 7C

Figure 7-3 Extended data and statistics for Figure 7D, E.

Figure 7-4 Extended data and statistics for Figure 7G, H.

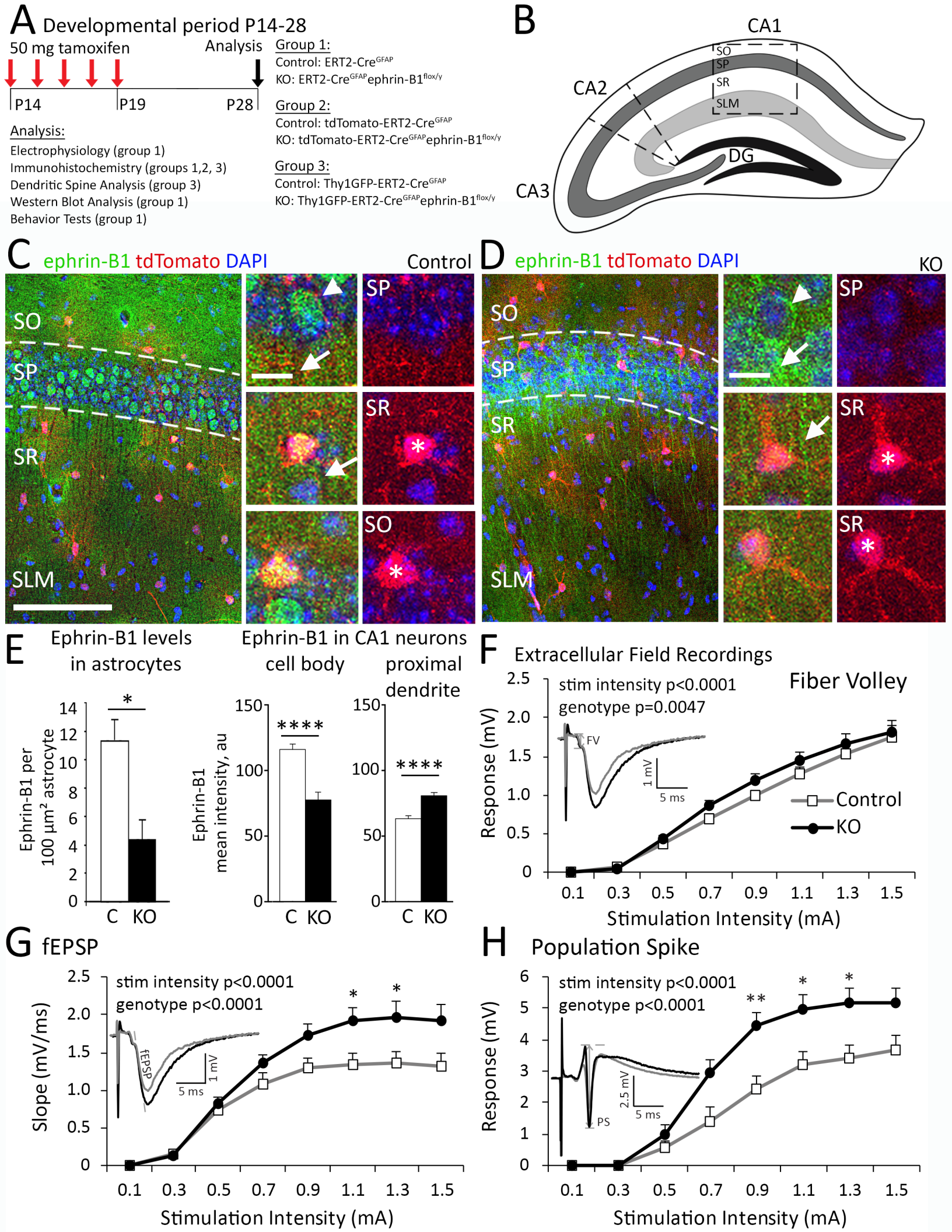
A Developmental period P14-28
50 mg tamoxifen
Analysis
P14
P19
P28
Analysis:
Electrophysiology (group 1)
Immunohistochemistry (groups 1,2, 3)
Dendritic Spine Analysis (group 3)
Western Blot Analysis (group 1)
Behavior Tests (group 1)
Group 1:
Control: ERT2-Cre GFAP
KO: ERT2-Cre GFAP ephrin-B1 flox/y
Group 2:
Control: tdTomato-ERT2-Cre GFAP
KO: tdTomato-ERT2-Cre GFAP ephrin-B1 flox/y
Group 3:
Control: Thy1GFP-ERT2-Cre GFAP
KO: Thy1GFP-ERT2-Cre GFAP ephrin-B1 flox/y
B
CA1
CA2
CA3
DG
SO
SP
SR
SLM
C ephrin-B1 tdTomato DAPI
Control
D ephrin-B1 tdTomato DAPI
KO
E
Ephrin-B1 levels in astrocytes
Ephrin-B1 per 100 µm² astrocyte
Ephrin-B1 in CA1 neurons
cell body
proximal dendrite
Ephrin-B1 mean intensity, au
C KO
F Extracellular Field Recordings
Fiber Volley
stim intensity p<0.0001
genotype p=0.0047
FV
1 mV
5 ms
Control
KO
Response (mV)
Stimulation Intensity (mA)
G fEPSP
stim intensity p<0.0001
genotype p<0.0001
fEPSP
Slope (mV/ms)
H Population Spike
PS
2.5 mV
Response (mV)

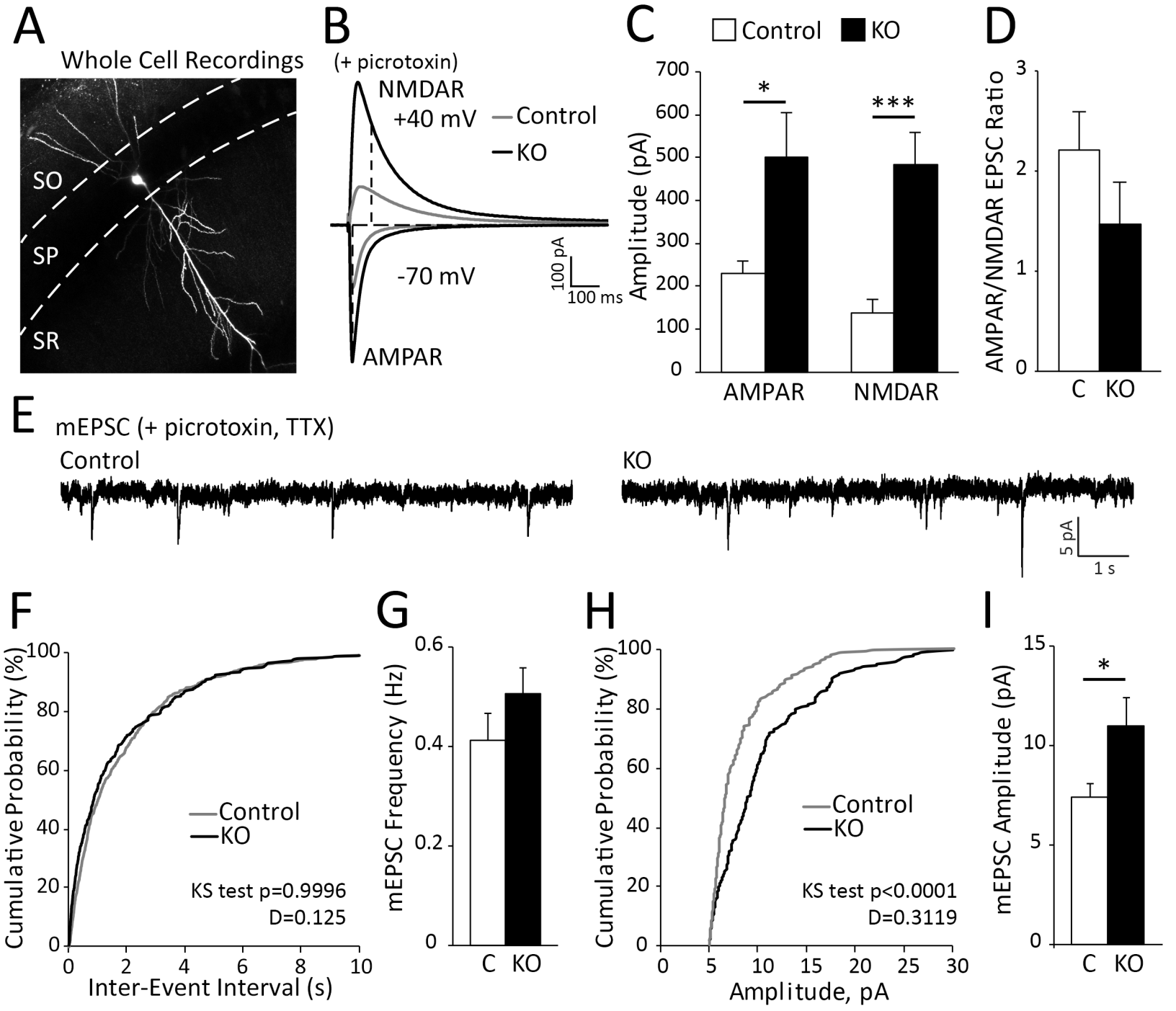
A
Whole Cell Recordings
SO
SP
SR
B
(+ picrotoxin)
NMDAR
+40 mV
Control
KO
-70 mV
AMPAR
100 pA
100 ms
C
Control
KO
Amplitude (pA)
*
***
AMPAR
NMDAR
D
AMPAR/NMDAR EPSC Ratio
C
KO
E
mEPSC (+ picrotoxin, TTX)
Control
KO
5 pA
1 s
F
Cumulative Probability (%)
Control
KO
KS test p=0.9996
D=0.125
Inter-Event Interval (s)
G
mEPSC Frequency (Hz)
C
KO
H
Cumulative Probability (%)
Control
KO
KS test p<0.0001
D=0.3119
Amplitude, pA
I
mEPSC Amplitude (pA)
*
C
KO

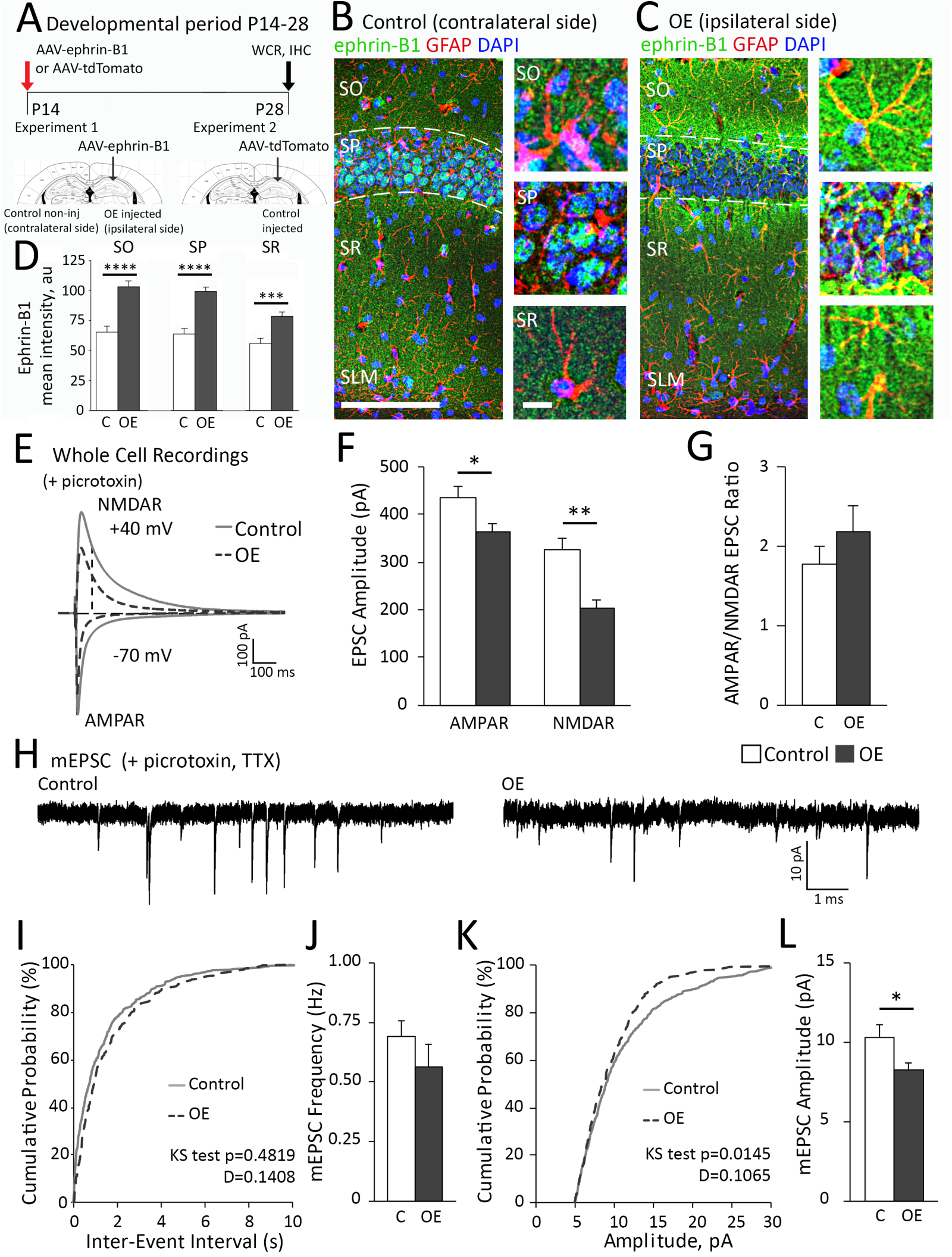
A Developmental period P14-28
AAV-ephrin-B1
or AAV-tdTomato
WCR, IHC
P14
P28
Experiment 1
Experiment 2
AAV-ephrin-B1
AAV-tdTomato
Control non-inj
(contralateral side)
OE injected
(ipsilateral side)
Control
injected
B Control (contralateral side)
ephrin-B1 GFAP DAPI
C OE (ipsilateral side)
ephrin-B1 GFAP DAPI
SO
SP
SR
SLM
D
SO
SP
SR
Ephrin-B1
mean intensity, au
125
100
75
50
25
0
****
****
***
C OE
C OE
C OE
E Whole Cell Recordings
(+ picrotoxin)
NMDAR
+40 mV
Control
OE
-70 mV
AMPAR
100 pA
100 ms
F
EPSC Amplitude (pA)
500
400
300
200
100
0
*
**
AMPAR
NMDAR
G
AMPAR/NMDAR EPSC Ratio
3
2
1
0
C OE
Control
OE
H mEPSC (+ picrotoxin, TTX)
Control
OE
10 pA
1 ms
I
Cumulative Probability (%)
100
80
60
40
20
0
Control
OE
KS test p=0.4819
D=0.1408
0 2 4 6 8 10
Inter-Event Interval (s)
J
mEPSC Frequency (Hz)
1.00
0.75
0.50
0.25
0
C OE
K
Cumulative Probability (%)
100
80
60
40
20
0
Control
OE
KS test p=0.0145
D=0.1065
0 5 10 15 20 25 30
Amplitude, pA
L
mEPSC Amplitude (pA)
15
10
5
0
*
C OE

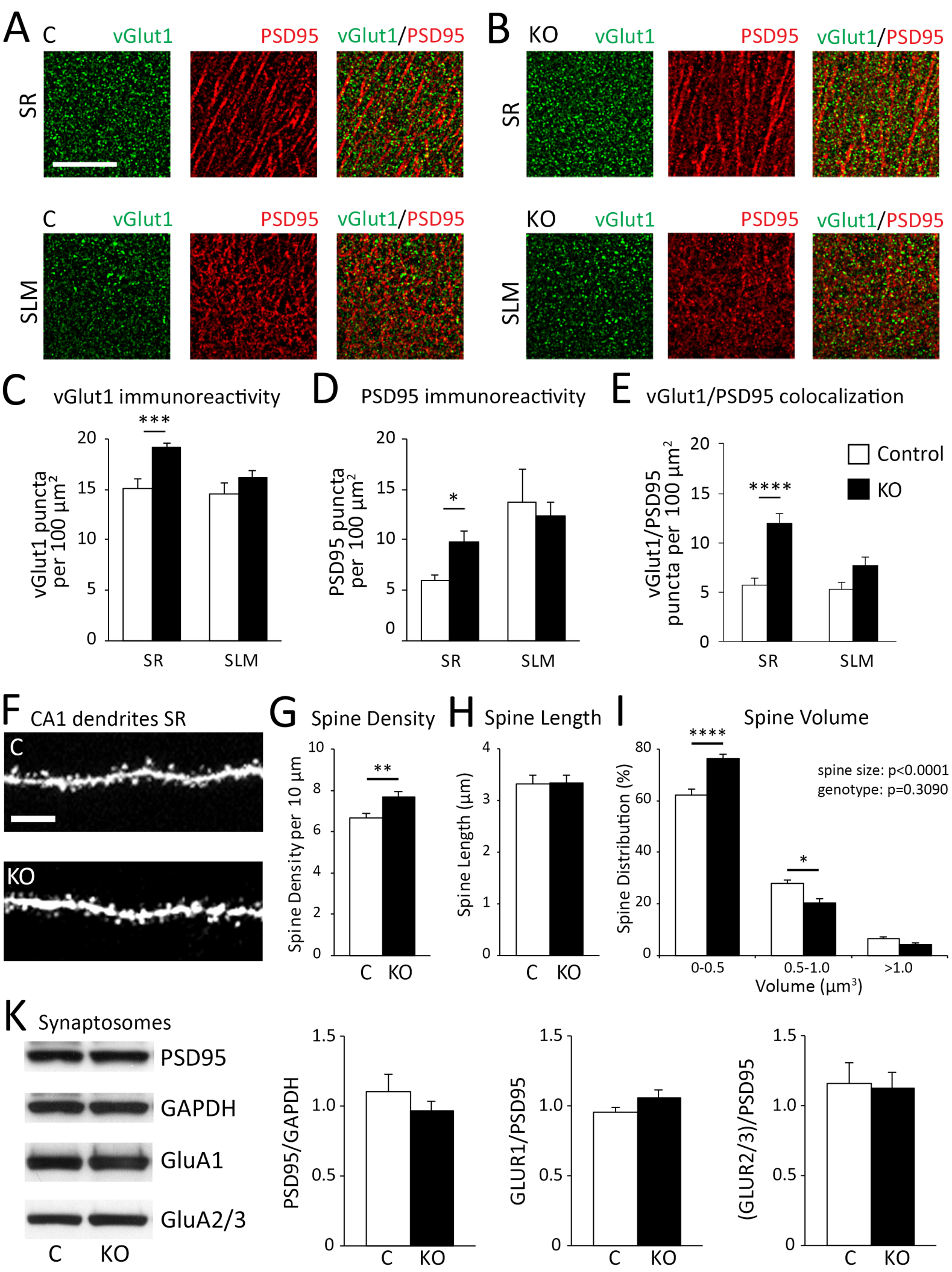
A
C
vGlut1
PSD95
vGlut1/PSD95
SR
SLM
B
KO
C
vGlut1 immunoreactivity
vGlut1 puncta per 100 µm²
***
SR
SLM
D
PSD95 immunoreactivity
PSD95 puncta per 100 µm²
*
E
vGlut1/PSD95 colocalization
vGlut1/PSD95 puncta per 100 µm²
****
Control
KO
F
CA1 dendrites SR
G
Spine Density
Spine Density per 10 µm
**
H
Spine Length
Spine Length (µm)
I
Spine Volume
Spine Distribution (%)
spine size: p<0.0001
genotype: p=0.3090
0-0.5
0.5-1.0
>1.0
Volume (µm³)
K
Synaptosomes
PSD95
GAPDH
GluA1
GluA2/3
PSD95/GAPDH
GLUR1/PSD95
(GLUR2/3)/PSD95

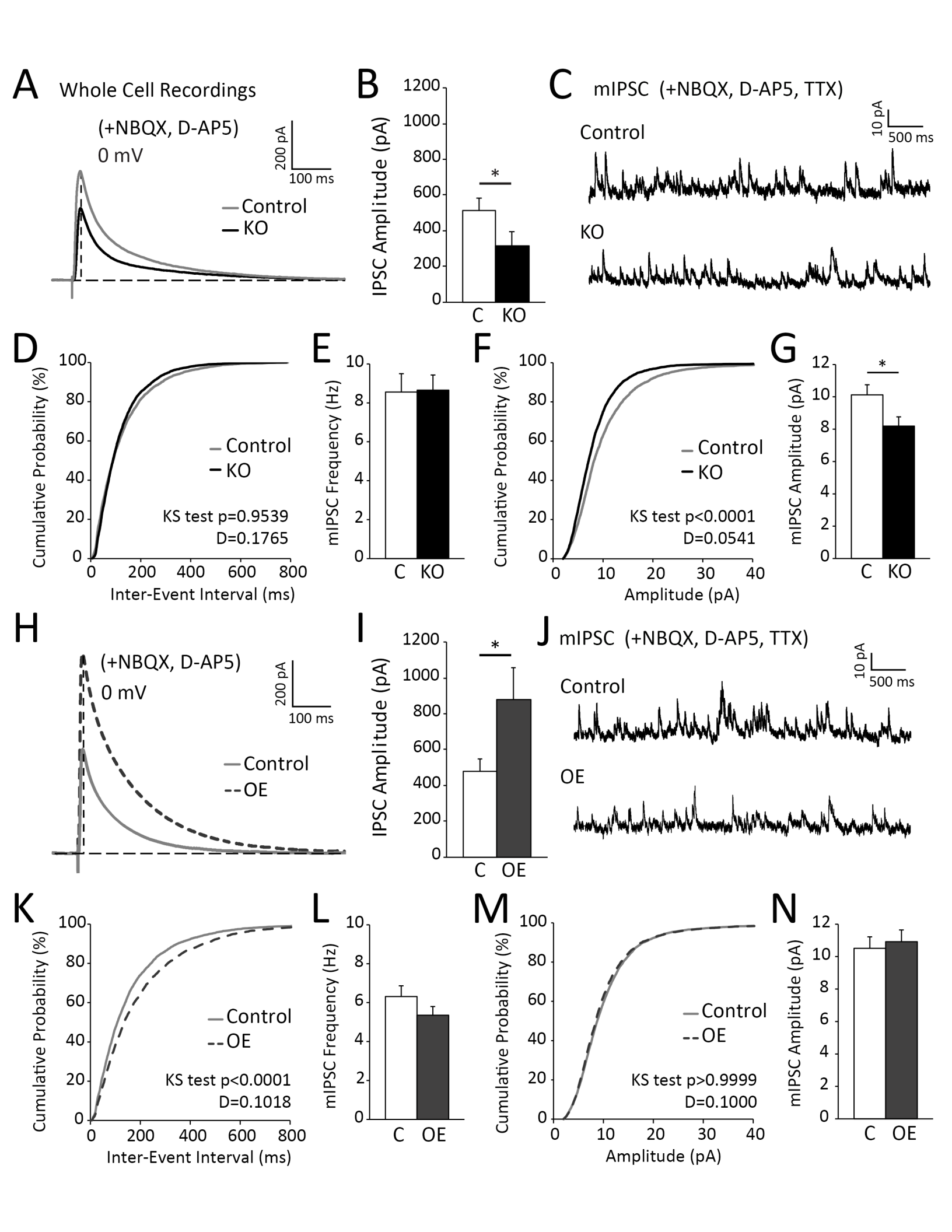
A
Whole Cell Recordings
(+NBQX, D-AP5)
0 mV
200 pA
100 ms
Control
KO
B
IPSC Amplitude (pA)
1200
1000
800
600
400
200
0
*
C
KO
C
mIPSC (+NBQX, D-AP5, TTX)
Control
KO
10 pA
500 ms
D
Cumulative Probability (%)
100
80
60
40
20
0
Control
KO
KS test p=0.9539
D=0.1765
0
200
400
600
800
Inter-Event Interval (ms)
E
mIPSC Frequency (Hz)
10
8
6
4
2
0
C
KO
F
Cumulative Probability (%)
Control
KO
KS test p<0.0001
D=0.0541
0
10
20
30
40
Amplitude (pA)
G
mIPSC Amplitude (pA)
12
10
8
6
4
2
0
*
C
KO
H
(+NBQX, D-AP5)
0 mV
200 pA
100 ms
Control
OE
I
IPSC Amplitude (pA)
1200
1000
800
600
400
200
0
*
C
OE
J
mIPSC (+NBQX, D-AP5, TTX)
Control
OE
10 pA
500 ms
K
Cumulative Probability (%)
Control
OE
KS test p<0.0001
D=0.1018
Inter-Event Interval (ms)
L
mIPSC Frequency (Hz)
C
OE
M
Cumulative Probability (%)
Control
OE
KS test p>0.9999
D=0.1000
Amplitude (pA)
N
mIPSC Amplitude (pA)
C
OE

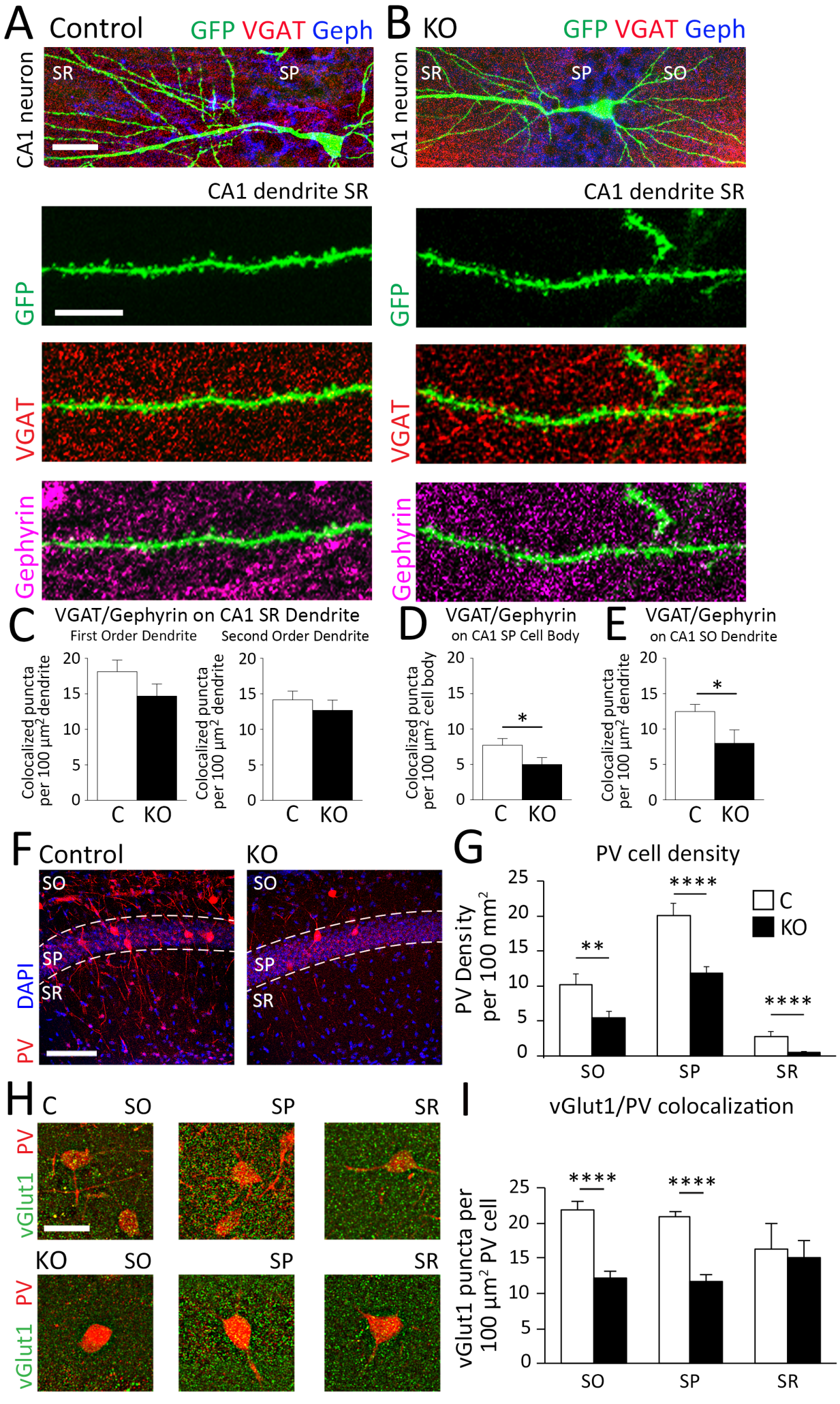
A Control
GFP VGAT Geph
CA1 neuron
SR
SP
B KO
GFP VGAT Geph
CA1 neuron
SR
SP
SO
CA1 dendrite SR
GFP
VGAT
Gephyrin
CA1 dendrite SR
GFP
VGAT
Gephyrin
C
VGAT/Gephyrin on CA1 SR Dendrite
First Order Dendrite
Second Order Dendrite
Colocalized puncta per 100 µm² dendrite
C
KO
D
VGAT/Gephyrin on CA1 SP Cell Body
Colocalized puncta per 100 µm² cell body
E
VGAT/Gephyrin on CA1 SO Dendrite
Colocalized puncta per 100 µm² dendrite
F Control
KO
SO
SP
SR
DAPI
PV
G
PV cell density
PV Density per 100 mm²
C
KO
SO
SP
SR
H C
KO
SO
SP
SR
PV
vGlut1
I
vGlut1/PV colocalization
vGlut1 puncta per 100 µm² PV cell
SO
SP
SR

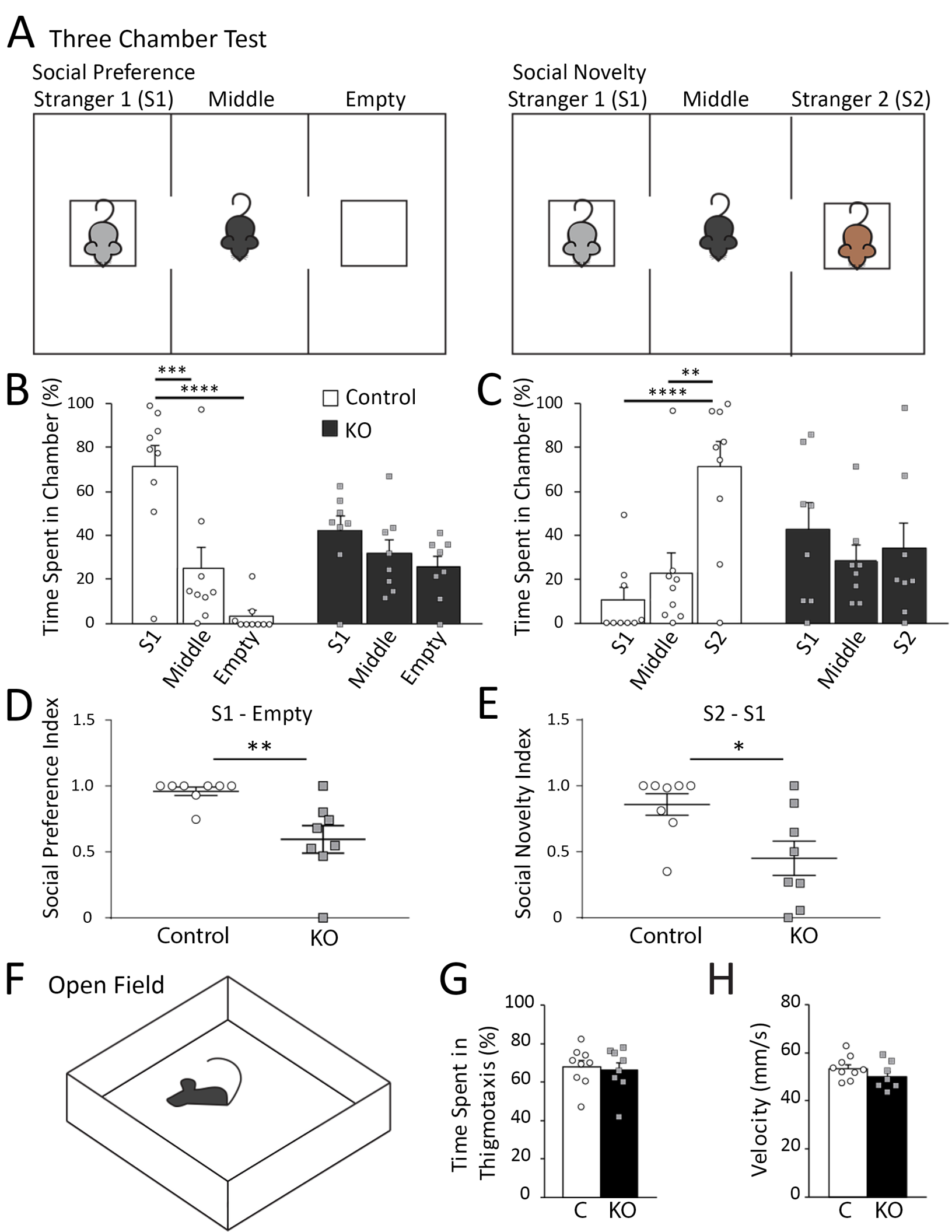
A
Three Chamber Test
Social Preference
Stranger 1 (S1)
Middle
Empty
Social Novelty
Stranger 1 (S1)
Middle
Stranger 2 (S2)
B
Time Spent in Chamber (%)
***
****
Control
KO
S1
Middle
Empty
C
Time Spent in Chamber (%)
**
****
S1
Middle
S2
D
Social Preference Index
S1 - Empty
**
Control
KO
E
Social Novelty Index
S2 - S1
*
Control
KO
F
Open Field
G
Time Spent in Thigmotaxis (%)
C
KO
H
Velocity (mm/s)
C
KO

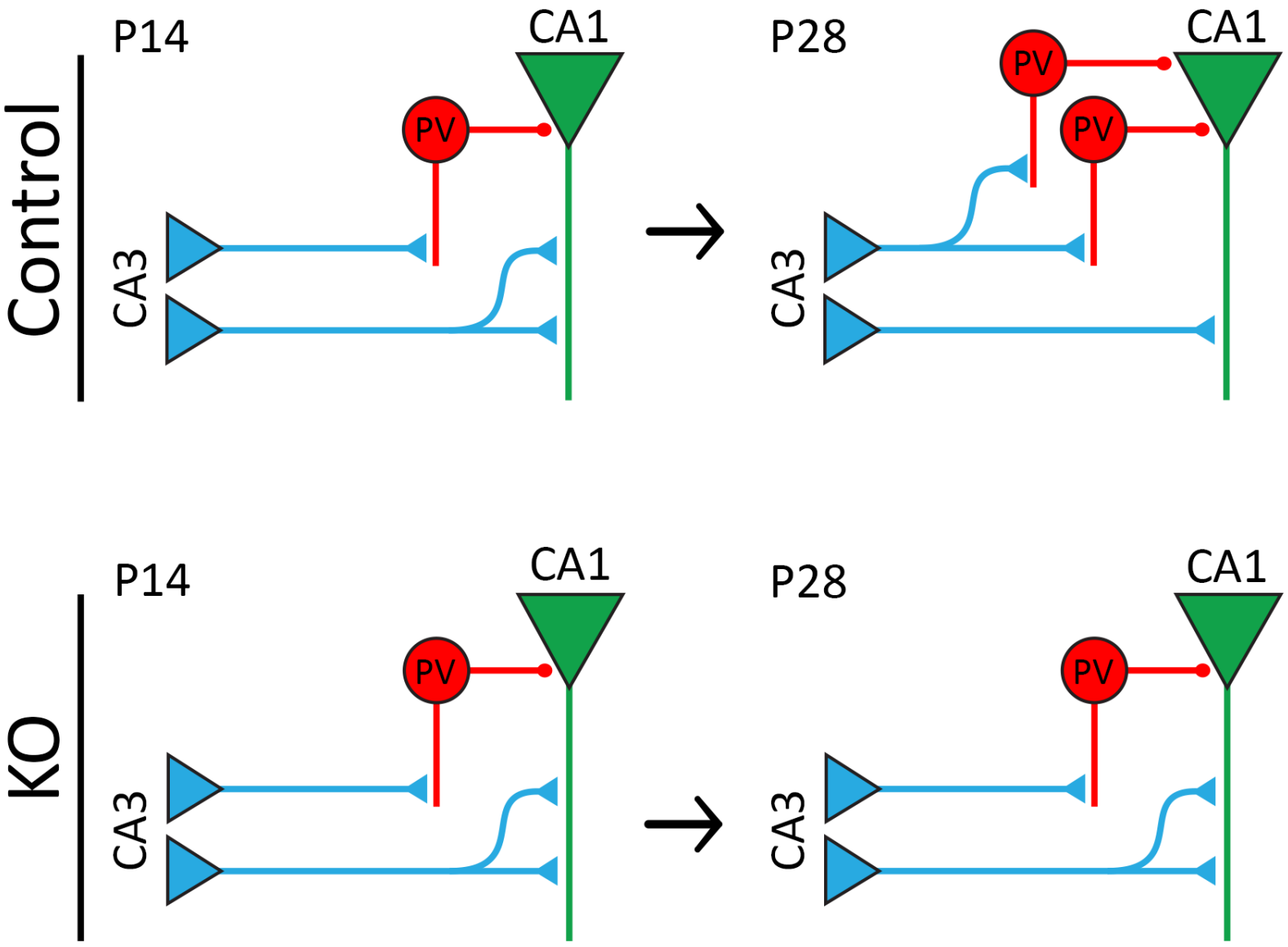
Control
P14
CA1
PV
CA3
P28
CA1
PV
PV
CA3
KO
P14
CA1
PV
CA3
P28
CA1
PV
CA3